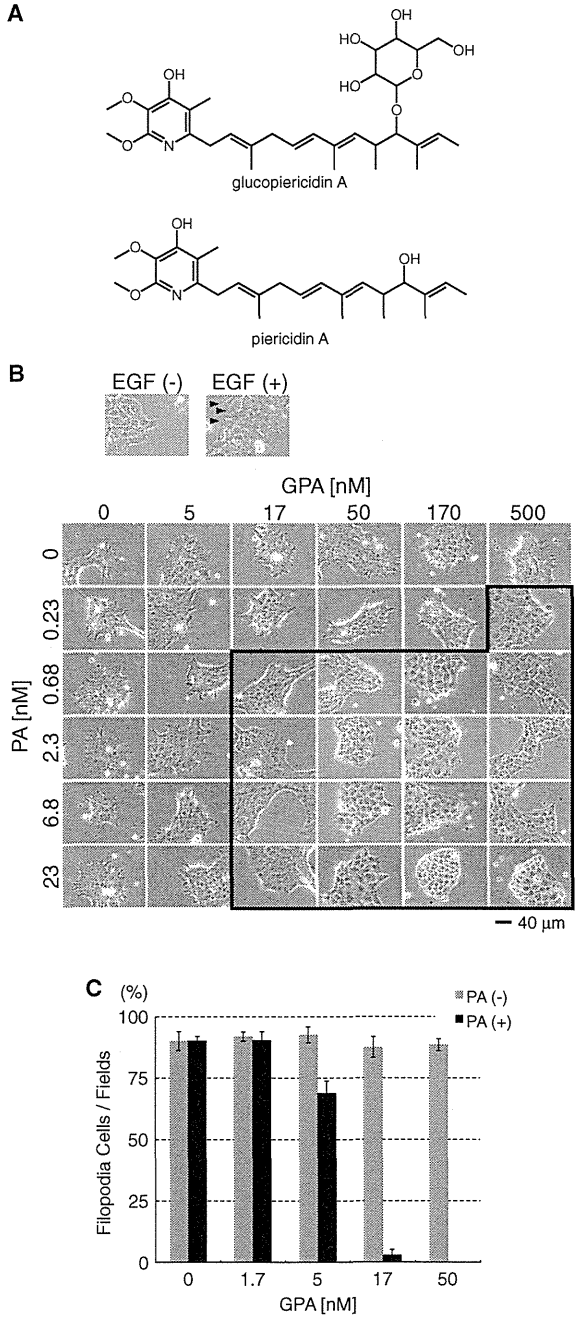

Figure 1. Synergistic Inhibition of Filopodia Protrusion by Cotreatment with GPA and PA

(A) Planar structures of GPA and PA.

(B) Synergistic inhibitory activity of GPA and PA in combination against filopodia protrusion in A431 cells. Cells were treated with varied concentrations of PA and GPA for 30 min and then stimulated by EGF (30 ng ml^{-1}) for 30 min to protrude filopodia (as shown by arrowheads in control picture above). Frameless photos indicate cells with filopodia, while the framed photos indicate cells in which filopodia protrusion was inhibited. Note that cotreatment with GPA and PA inhibited filopodia protrusion while single treatment with each did not, indicating that GPA and PA act synergistically. Photos represent the results of three independent experiments.

(C) Quantification of inhibition of filopodia protrusion by GPA and PA cotreatment. The number of A431 colonies with filopodia were determined microscopically, and the rate of inhibition [filopodia colonies] / [total colonies] in a field was calculated. Error bars represent ± SD (n = 9). The same result was obtained in duplicate.

See also Figure S1 and Table S1 for the supporting data on the bioassay-guided isolation, the structural identification, and the bioactivity of GPA and PA.

and NMR as piericidin A (PA) (Hall et al., 1966) (Figure 1A). The final purification procedure is described in Figure S1E.

Next, we examined the inhibitory activity of GPA and PA against filopodia protrusion (Figures 1B and 1C). Neither GPA nor PA alone, at concentrations up to 500 nM and 2.3 μM, respectively, showed inhibitory activity (see also Figure S1F). When combined, however, much lower concentrations of GPA (17 nM) and PA (0.68 nM) produced inhibition of filopodia protrusion. Hence, we isolated two natural products that inhibit EGF-induced filopodia protrusion in a synergistic manner.

PA-Mediated Inhibition of Mitochondrial Respiration Is Necessary for Inhibition of Filopodia Protrusion

Next, we investigated the mechanisms underlying the synergistic inhibition of filopodia protrusion using cotreatment with GPA and PA. Since PA is a known inhibitor of the mitochondrial respiratory chain complex I (Gutman et al., 1970; Hall et al., 1966), we hypothesized that inhibition of mitochondrial respiration by PA was required for the observed synergistic inhibition of filopodia protrusions when cells were cotreated with GPA and PA. To test this hypothesis, we examined whether other inhibitors of mitochondrial respiration would inhibit filopodia protrusion in combination with GPA. As expected, rotenone, another complex I inhibitor, showed the synergistic inhibition in combination with GPA (Figure 2A). In addition, antimycin A, a mitochondrial respiratory chain complex III inhibitor, and oligomycins, complex V inhibitors, also inhibited filopodia protrusion synergistically with GPA (Figure 2A). These results suggested that suppression of mitochondrial respiration is responsible for the synergistic filopodia inhibition seen with GPA and PA. Conversely, although GPA is the glucopyranoside derivative of PA, GPA showed low inhibitory activity against mitochondrial respiration (about 500-fold weaker than PA) (see Figure S2). The weak inhibition of mitochondrial respiration suggested that GPA must contribute to inhibition of filopodia protrusion through a different mode of action.

Elucidating GPA's Mode of Action through CE-MS Metabolomics

We conducted chemical genomic screening to investigate the mode of action whereby GPA contributes to the inhibition of filopodia protrusion. In this screening, the biological profile of target-identified inhibitors of filopodia inhibition was compared with that of GPA in order to find target-identified inhibitors with the same bioactivity as GPA, considering the possibility that GPA might target the same molecules as these other inhibitors. About 200 target-identified compounds were assessed for their ability to inhibit EGF-induced filopodia protrusion in the presence of PA (Table S2). As a result of this analysis, we found that 2-deoxyglucose (2DG), a known suppressor of glycolysis (Bachelard et al., 1971), was the sole compound able to inhibit protrusion in combination with PA (Figure 2B).

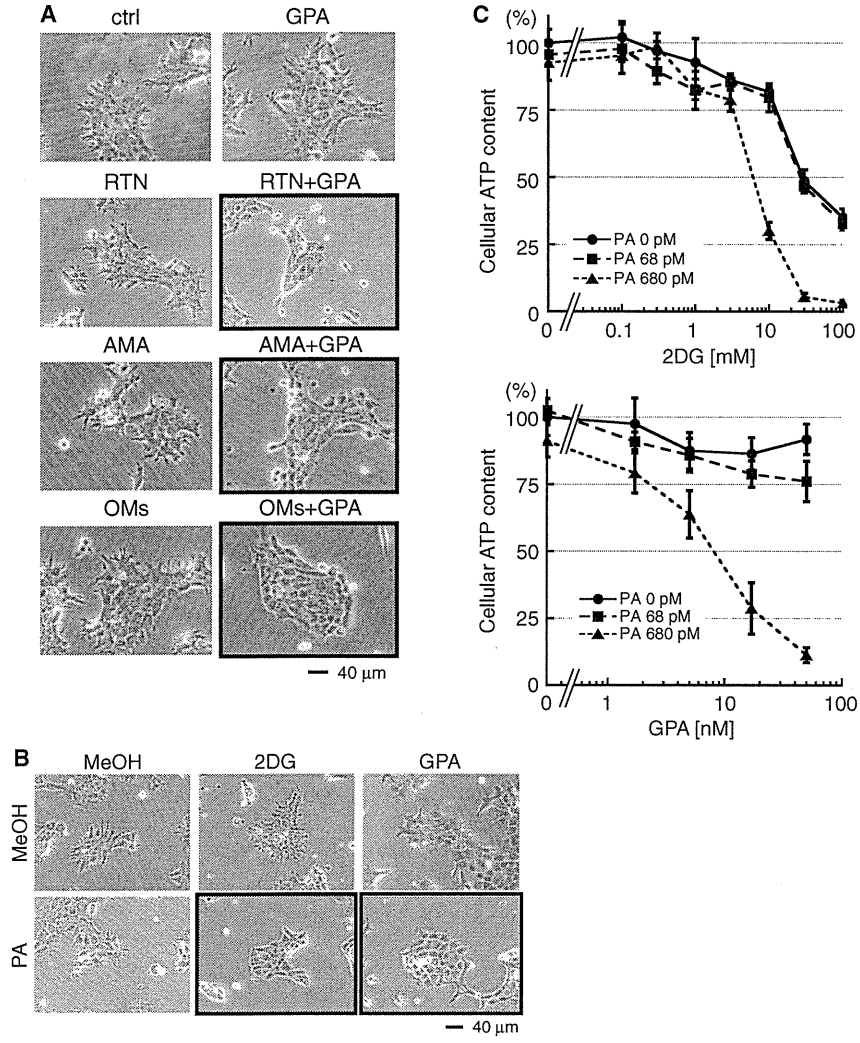

Figure 2. Mechanistic Insights into Synergistic Inhibition of Filopodia Protrusion by GPA and PA

(A) Synergistic inhibition of filopodia protrusion by inhibitors of mitochondrial respiration in the presence of GPA. Mitochondrial inhibitors with similar activity to PA also inhibited filopodia protrusion in the presence of GPA. Mitochondrial inhibitors RTN (rotenone: another inhibitor of complex I), AMA (antimycin A: complex III inhibitor), and OM (oligomycins: complex V inhibitor) were used.

(B and C) GPA appears to suppress glycolysis. Through chemical genomic screening of target-identified inhibitors, we found that the hexokinase inhibitor 2DG alone synergistically inhibited filopodia protrusion in the presence PA, similar to the effect observed with GPA (for B) the entire screening results are shown in Table S2). Since hexokinase inhibition by 2DG would suppress glycolysis, this suggested that glycolytic suppression might be responsible for the synergistic inhibition of filopodia protrusion with PA, and that therefore GPA might also suppress glycolysis. This validity of this hypothesis was supported by the result demonstrating that GPA decreases cellular ATP in the presence of the mitochondrial respiration inhibitor PA (C), since it is known that glycolytic suppression causes a drastic decrease in cellular ATP under the suppression of mitochondrial respiration. Error bars: SD (n = 3).

The respiratory inhibition by PA and the weak inhibition by GPA are shown in Figure S2.

This raised the possibility that glycolytic suppression could be involved in the synergistic inhibition of filopodia protrusion seen with PA. Additionally, filopodia protrusion has been described as an ATP-dependent process (Le Clainche and Carlier, 2008). Thus, we hypothesized that PA and 2DG inhibit filopodia protrusion by decreasing cellular ATP levels through simultaneous blockage of two ATP-producing metabolic pathways: glycolysis (2DG) and mitochondrial respiration (PA). In support of this hypothesis, we found that 2DG did indeed decrease cellular ATP levels synergistically with PA (Figure 2C). We therefore suspected that GPA might also decrease cellular ATP levels, resulting in inhibition of filopodia protrusion in the same manner as 2DG. As shown in Figure 2C, treatment of A431 cells with GPA also caused a drastic decrease in cellular ATP with PA, suggesting that GPA might perturb the ATP-producing metabolic pathways, most likely glycolysis, resulting in the filopodia protrusion inhibition in the presence of PA.

One possible approach to address the issue of whether GPA actually perturbs glycolysis is to assess the effect of GPA on global metabolism and on glycolysis in particular, by measuring the metabolome using CE-TOFMS. In CE-TOFMS, metabolites are separated by capillary electrophoresis (CE) on the basis of their charge and size, and then detected as peaks in MS (Soga et al., 2003). Metabolites are identified by comparing CE migration time and molecular weight with that of standards, and are quantified by peak intensity in reference to standard calibration curves. We used this approach to quantitatively examine the differences in metabolite levels between control and GPA-treated cells.

Using the CE-TOFMS approach, we detected around 4000 (3853–4848) peaks in each sample (control and GPA-treated, n = 4). A reference set of 112 standards was used to identify the metabolites of glycolysis and related pathways (pentose phosphate pathway, TCA cycle, nucleotide synthesis, amino acid, and others, see Figure 3). A total of 83 peaks were quantitatively identified, and 24 metabolites were found to significantly differ between control and GPA-treated samples (for the entire list with exact p values, see Table S3), which are mapped in the overview in Figure 3 (pathway information was obtained by reference to KEGG [http://www.genome.jp/kegg/pathway.html]).

Our results showed that GPA significantly decreased the amount of glycolytic end products (pyruvate: 61.5%, $p = 3.8 \times 10^{-5}$ and lactate: 40.3%, $p = 1.4 \times 10^{-5}$). Moreover, another glycolytic parameter, the lactate/pyruvate ratio, was also

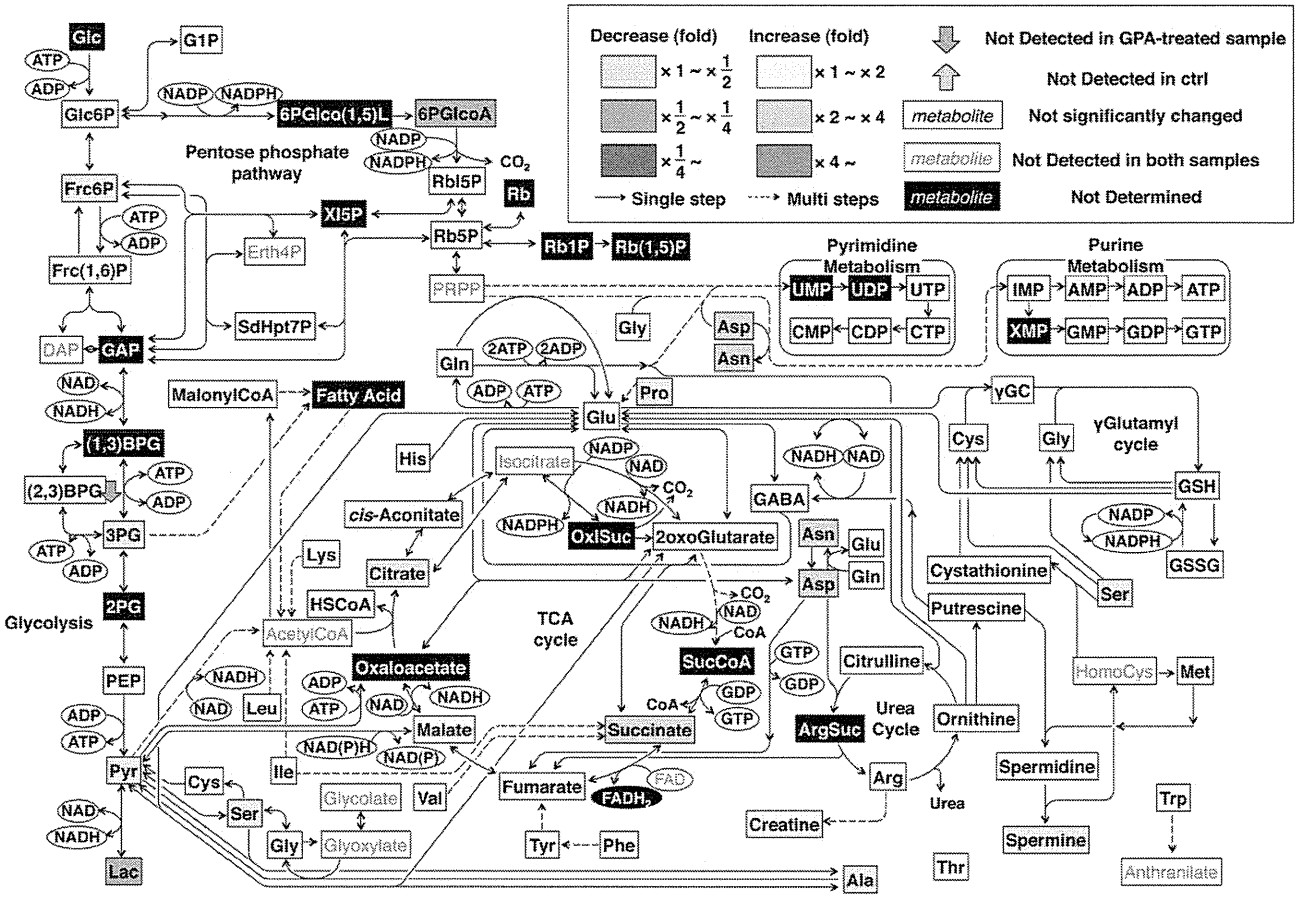

Figure 3. Snapshot Picture of GPA-Changed Metabolome

The global metabolites in GPA-treated A431 cells (30 min treatment) were extracted and analyzed by CE-TOFMS, and compared with that of control cells. Significantly decreased metabolites in GPA-treated cells are shown as □, ▨, and ■ (fold decrease >50%, >25%, and <25%, respectively), and significantly increased metabolites are shown as □, ▨, and ■ (fold increase <200%, <400%, and >400%, respectively). Significance was determined by Student's t test ($n = 4$, $p < 0.05$). The entire set of results with exact p values and list of metabolite abbreviations are listed in Table S3. (See also Figure S3 for lactate/pyruvate ratio.)

significantly decreased (Figure S3). These results strongly suggested that GPA-inhibited glycolysis.

GPA Targets Glucose Uptake

Upon determining that GPA inhibits glycolysis, we then examined which reaction step in glycolysis was blocked by GPA as a means of identifying the GPA target. To reveal particular GPA-induced changes in glucose metabolism, control and GPA-treated A431 cells were treated with [1,2,3,4,5,6-^{13}C]-glucose (full-label), and then the [^{13}C]-incorporated metabolites within those cells were quantified by CE-MS. Incorporation of [^{13}C]-labeled glucose into any metabolites of glycolysis was decreased in GPA-treated cells (Figure 4; Table S4), indicating that the glycolytic influx was lowered by GPA treatment. Since the metabolite closest to glucose in the glycolytic pathway is glucose-6-phosphate (G6P), these results suggest that GPA acts on the steps proceeding from glucose uptake to G6P production.

Since hexokinase catalyzes G6P production, we examined the effect of GPA on hexokinase activity in vitro. Glucose, as a substrate of hexokinase, was mixed with reaction buffer containing partially purified hexokinase, G6PDH, and NADP as a coenzyme of the G6PDH reaction, and incubated at room temperature (Bergmeyer, 1963; Floridi et al., 1981). In this reaction, the G6P produced by hexokinase is further hydrolyzed by G6PDH, with the accompanying conversion of NADP to NADPH, so that hexokinase activity can be estimated by the spectrophotometric absorbance of NADPH (Bergmeyer, 1963). As shown in Figure 5A, the assay revealed that addition of glucose led to an increase in the amount of NADPH, which could be negated by the hexokinase inhibitor 2DG. However, GPA at concentrations up to 1.7 μM failed to inhibit the reaction, indicating that the hexokinase reaction step is not the point of inhibition of glycolysis through a decrease in the amount of G6P by GPA.

Another possible step that GPA could act upon to cause a decrease in G6P is glucose uptake. To examine this possibility, we treated cells with [^{3}H]-2DG and evaluated whether GPA would affect glucose uptake. The compound 2DG acts as a glucose mimic and is incorporated into cells by glucose transporters. However, 2DG cannot be catabolized in glycolysis; thus, the amount of 2DG that is taken up simply reflects the glucose uptake capacity of a cell's glucose transporters.

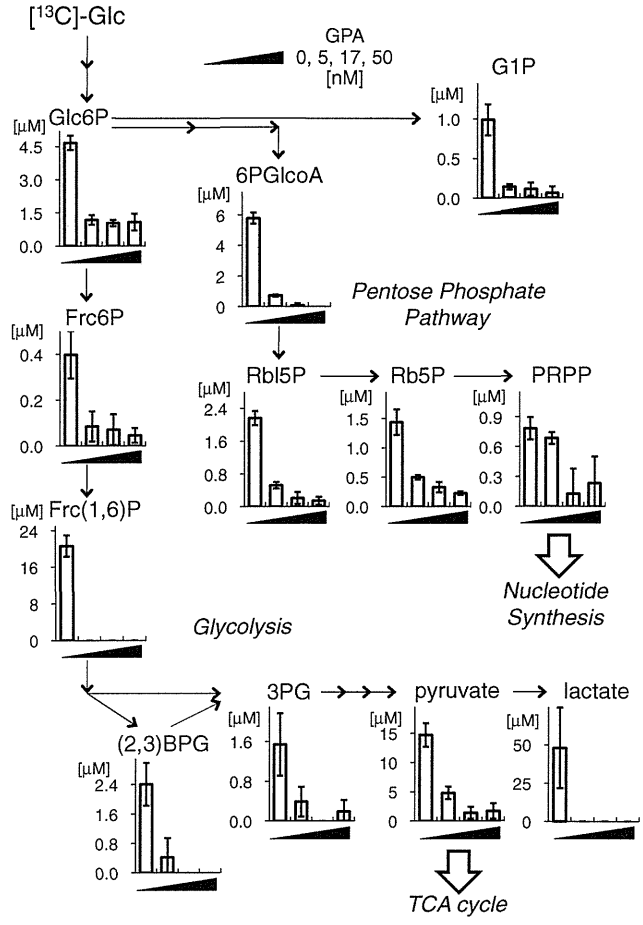

Figure 4. [^{13}C]-Labeling Study

[^{13}C]-glucose was incorporated into A431 cells for 30 min immediately after GPA treatment. All detected major isotopomers ([^{13}C]-glucose-6-phosphate and its [^{13}C]-metabolites) were decreased by GPA treatment (the entire list is shown in Table S4), indicating that GPA inhibits the step from [^{13}C]-glucose uptake to [^{13}C]-glucose-6-phosphate production. Error bars: SD (n = 4).

In our experiments, GPA inhibited the uptake of [^{3}H]-2DG in a dose dependent manner (Figure 5B), with an IC_{50} of 4.9 ± 2.9 nM (mean ± SE, n = 3). This concentration was quite similar to the concentration of GPA required to inhibit EGF-induced filopodia protrusion in combination with PA (Figures 1B and 1C). It is reported that GLUT1 is responsible for glucose uptake in A431 cells (Aloj et al., 1999). Treatment of cells with GPA did not change the expression level of GLUT1 in the plasma membrane (Figure S5A), which suggests that GPA inhibits GLUT1 function.

To confirm whether GPA does in fact inhibit GLUT1 function, GLUT1 was overexpressed in cells (Figure S5B), and the sensitivity of cells to GPA upon 2DG uptake was evaluated. Uptake of 2DG was substantially increased (about 4-fold) by GLUT1 overexpression (expression level was shown in Figure S5B). Although GPA could inhibit 2DG uptake in GLUT1-overexpressing cells, when compared with vector control cells, GLUT1-overexpressing cells became less sensitive to GPA depending on the expression level of GLUT1 (Figure 5C). The IC_{50} value for 2DG uptake increased with GLUT1 expression (21.6 ± 7.7 nM, [mean ± SE, n = 3) in vector control cells versus 108 ± 24 nM (mean ± SE, n = 3) in GLUT1-overexpressing cells). These results indicated that GPA inhibits GLUT1 function, and thereby inhibits glycolysis.

DISCUSSION

In this study, we conducted natural product screening to isolate the inhibitor of EGF-induced filopodia protrusion. Natural products have historically provided a variety of important bioactive compounds, such as antibiotics, immunosuppresants, and antitumor agents (Abel et al., 2002; Lokey, 2003; Newman and Cragg, 2007). Natural product screening has also led to discovery of unique bioactive compounds useful in chemical genetic research (e.g., FK506 [Liu et al., 1991] and lactacystin [Fenteany et al., 1995]). Natural products often contain unique structures and chiral centers, which anecdotal evidence suggests are important for the unique bioactivity and target recognition of many compounds. We therefore conducted natural product screening in microorganisms to isolate and characterize an inhibitor of filopodia protrusion.

As a result of our screening studies, we found that the cultured broth of *Lechevalieria sp.* strain 1869-19 contained compounds that inhibited EGF-induced filopodia protrusion (Figure 1A). However, this inhibition required the synergistic effect of two compounds (Figures S1D and S1E), which were isolated and identified as GPA and PA (Figures 1A–1C).

We then examined the mechanism underlying the synergistic inhibition of filopodia protrusion caused by GPA and PA. PA is a well-known inhibitor of respiratory complex I in mitochondria (Gutman et al., 1970). Because other mitochondrial respiratory inhibitors, such as antimycin A and oligomycins, inhibited filopodia protrusion only in the presence of GPA, inhibition of mitochondrial respiration by PA could be responsible for the synergistic inhibition of GPA and PA (Figure 2A). Little is known about GPA however. There are few reports in the literature that describe the biological activities of GPA (Ahn et al., 1995; Matsumoto et al., 1987), and its molecular target(s) and mode of action have not been determined. To address this issue, we employed a chemical genomic approach, in which a target-identified chemical library was searched to find compounds with activity similar to GPA. The compound 2-deoxy-glucose (2DG) was identified using this approach (Figure 2B; Table S2).

Because 2DG is known to inhibit glycolysis by inhibiting the enzyme hexokinase, GPA would be expected to also inhibit glycolysis. By means of metabolomic analysis using CE-TOFMS (Figure 3) in combination with an evaluation of [^{13}C]-labeled glycolytic metabolites (Figure 4), we clearly determined that GPA disrupts glycolysis by inhibiting the initial step of the pathway. Finally, we have also clarified that glucose transporters are functional target proteins of GPA (Figure 5).

Glucose transporters comprise a large family of transmembrane proteins characterized by having different affinities for glucose (Mueckler et al., 1985; Scheepers et al., 2004). Among glucose transporters, GLUT1 has a high affinity for glucose and is one of the most abundantly expressed transporters in many types of tumors (Scheepers et al., 2004). Indeed, A431 cells used in this study have been reported to express only

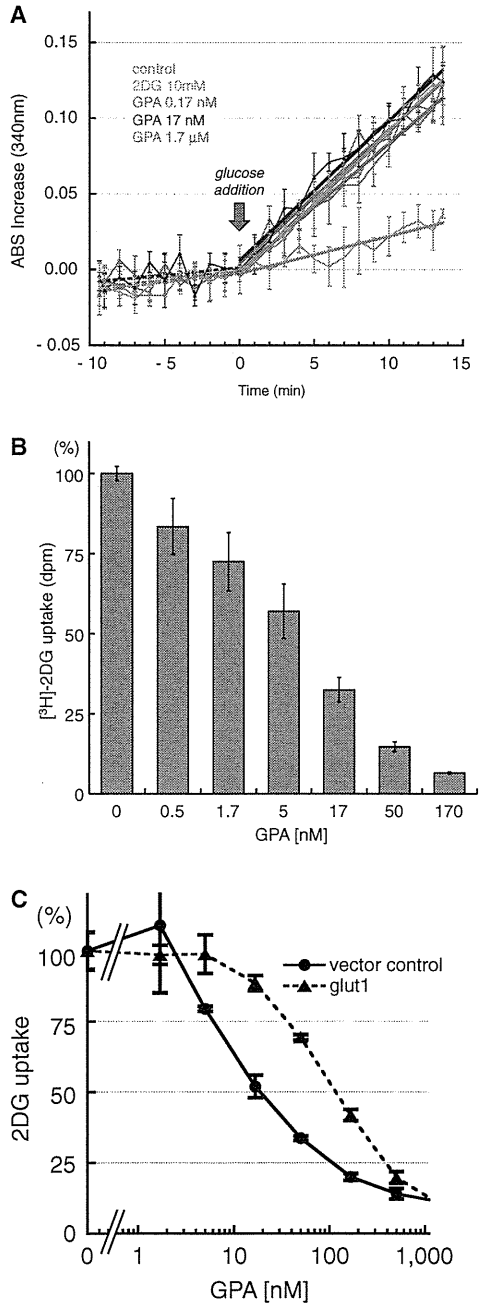

Figure 5. GPA-Mediated Inhibition of Glucose Uptake via GLUT

(A) GPA failed to inhibit the in vitro hexokinase enzyme reaction. Previously, hexokinase activity was successfully monitored by addition of the hexokinase substrate glucose, causing an increase in enzymatic activity (detected by NADPH absorbance at 340 nm), which was inhibited by 2-deoxyglucose. However, GPA could not inhibit this increase in hexokinase activity, indicating that GPA was not a hexokinase inhibitor. Error bars: SD (n = 3).

(B) Inhibition of glucose uptake by GPA. GPA inhibited the uptake of the glucose mimic 2-deoxyglucose (2DG) in a dose-dependent manner. Error bars: SD (n = 3). Similar results were obtained from three individual experiments. These results explain the glucose-6-phosphate decrease depicted in Figure 4.

(C) Inhibition of GLUT1-mediated glucose uptake by GPA. Since glucose uptake in A431 cells is primarily mediated by GLUT1, A431 GLUT1 was overexpressed, and the sensitivity of glucose uptake to GPA was examined. Overexpression lowered the sensitivity 2DG uptake inhibition by GPA as observed with the shift of the inhibition curve to the right. Error bars: SD (n = 3). The data shown represent results of three independent experiments.

(See also Figure S5.)

GLUT1 as glucose transporter (Aloj et al., 1999). Therefore, data accumulated in this study suggest that there are only three likely mechanisms that could explain glucose uptake inhibition by GPA: (i) GPA mimics the GLUT1 substrate, (ii) inhibition of GLUT1 translocation into the cell membrane, and (iii) lowering the expression level of GLUT1. We ruled out the last two possibilities by immunoblotting, as shown in Figure S5A. The data showing that the level of GLUT1 expression was not changed in the membrane fraction by GPA treatment suggest that uptake inhibition by GPA was not due to an inhibition of GLUT1 translocation or a reduction in GLUT1 expression. Moreover, GPA possesses the glucose moiety, and glucose null derivative PA failed to inhibit the uptake (Figure S5C). Thus, it is likely that the glucose uptake inhibition by GPA would be due to its glucopyranoside moiety, perhaps by functioning as a glucose mimic to GLUT1. This suggests that GLUT1 would be the bona fide target of GPA due to GPA's inhibition of glycolysis in A431 cells.

Our overexpression study confirmed GPA inhibits glucose uptake via GLUT1 in A431 cells, but we also tested GPA against another glucose transporter, GLUT4 in Swiss 3T3 cells. Differentiated Swiss 3T3-L1 adipocytes take up glucose basally via GLUT1. However, when 3T3-L1 adipocytes are stimulated with insulin, GLUT4 is translocated to the membrane (Saito et al., 2007), and both GLUT1 and GLUT4 transport glucose into the cells. GPA inhibited both the basal uptake of [^{3}H]-2DG via GLUT1 and the increased uptake of glucose in insulin-stimulated cells (Figure S5D), suggesting that GPA inhibits glucose uptake via both GLUT1 and GLUT4.

The glucose transporter inhibitors cytochalasin B and phloritin are known to suppress glucose uptake at μM and mM concentrations, respectively. GPA, on the other hand, inhibits glucose uptake in A431 cells, Swiss 3T3-L1 adipocytes, and GLUT1-overexpressed HEK293T cells at nanomolar concentrations (Figures 5B and 5C; Figure S5D). Thus, ours is the first report to our knowledge of a GLUT inhibitor capable of suppressing glucose uptake at nanomolar concentrations.

Aside from its influence on glycolysis, GPA treatment also leads to changes in the amounts of TCA cycle intermediates, as well as increases in levels of aspartate and asparagine (Figure 3; Table S3). We believe these changes may be caused in a part by GPA-limited entry of pyruvate into the citrate cycle, which might slow the rate at which oxaloacetate is converted to citrate. Slowing the conversion of oxaloacetate may lead to accumulation of preceding TCA cycle intermediates such as malate, fumarate, and succinate.

Reports suggest that active glutaminolysis takes place in the metabolome of tumor cells (Deberardinis et al., 2007), described as anaplerotic ATP energy fueling through "truncated" TCA metabolism (from 2-oxoglurate to malate) without pyruvate entry (Parlo and Coleman, 1984; Piva and McEvoy-Bowe, 1998). In tumor glutaminolysis, highly incorporated glutamine is converted into glutamate and then into 2-oxoglutarate via aspartate transaminase, with production of aspartate as a byproduct

(Piva and McEvoy-Bowe, 1998). Thus, the possibility should not be excluded that these changes in the amounts of TCA cycle intermediates and aspartate are caused by glutaminolysis in addition to GPA-suppressed pyruvate entry into the TCA cycle (Kovacević et al., 1987).

CE-MS metabolome analysis is a powerful technique that may help elucidate the targets of the compounds, in the case the compounds impact glycolysis. Glutaminolytic analyses, and labeling studies using [^{13}C]-glutamine in combination with CE-TOFMS—analogous to our studies of GPA's effect on glycolytic pathways—might clarify the target-unverified compounds that disturb glutaminolysis. Chemical metabolomic analyses should therefore be encouraged, not only because they may further understanding of the physiological and pathological effects of many natural products, but also because such studies may enhance development of compounds that may serve as a new class of anticancer drugs which regulate the tumor metabolome.

An important question raised by our results is how the decrease in cellular ATP caused by the inhibition of glycolysis and mitochondrial respiration by GPA and PA cotreatment results in suppression of EGF-stimulated filopodia protrusions in A431 cells. The molecule Profilin may hold the key to this answer. Profilin is critical role for filopodia protrusion because it promotes polymerization of filamentous actin (F-actin) at the extending ends of filopodia (Witke, 2004).

Profilin binds to ADP-bound actin monomers, promotes exchange of ADP for ATP, and releases ATP-actin at the growing ends of F-actin, leading to polymerization of actin in a straight-lined form (Le Clainche and Carlier, 2008; Witke, 2004). The profilin-mediated elongation of F-actin bundles pushes the cell membrane outward, resulting in the protrusion of spike-shaped filopodia. In this regard, ATP provides the energy for Profilin-mediated filopodia protrusion. Moreover, Molitoris et al. observed that ATP depletion resulted in punctate dispersion of F-actin from its straight-lined form (Molitoris et al., 1991), suggesting that stabilization of straight-lined F-actin depends on the level of ATP in the cell. Therefore, one possible explanation for the inhibition of filopodia protrusion by GPA and PA cotreatment might be the lowering of intracellular ATP concentration caused by the blockage of glycolysis by GPA and mitochondrial respiration by PA.

Our study was based on the screening of crude natural products and bioassay-guided isolation of the components that inhibit filopodia protrusion. Recently, natural product screening has declined in popularity, probably because the isolation and structural determination steps are costly and time consuming. However, we believe our use of this technique to isolate compounds that act synergistically to inhibit an important cellular process demonstrate that crude natural product screening is still a valuable technique. Since cellular responses are driven by many complex systems that are often robust due to the presence of rescue and feedback pathways, the best strategy for finding bioactive inhibitors of a particular cellular system may be global screening of crude extracts of natural products. In conclusion, though the approach in this study may be deemed "old-fashioned" and somewhat laborious, we believe the results provided here have opened the broad avenue of natural products screening for the continued progress in chemical genetics research.

SIGNIFICANCE

This study began with the natural product screening to obtain the unique bioactive compounds. To obtain the unique bioactive compounds, filopodia seem a good target for the inhibitor screening from microbial origin because of few inhibitors in reports. Moreover, filopodia in tumor cells contribute to the metastasis; therefore, such inhibitor holds the therapeutic impacts for the tumor treatment. By screening the microbial broth, we found the cultured broth of one *Lechevalieria sp.* strain that inhibited the tumor filopodia protrusion. However, this inhibition disappeared following silica-gel chromatography. Interestingly, the inhibitory activity was almost completely recovered by remixing all of the silica-gel chromatography fractions, suggesting that the inhibition required the synergistic effect of two or more compounds contained within the microbial broth that eluted in different fractions. We tried to isolate the components responsible for inhibition of filopodia protrusion and found glucopiericidin A (GPA) and piericidin A (PA). PA is a known inhibitor of mitochondrial respiration, but the mode of action of GPA has not yet been reported. Our experiments with CE-TOFMS metabolomic analysis showed that GPA suppressed glycolysis and identified glucose transporters as the functional target molecule of GPA. Importantly, GPA is glucopyranoside derivative of mitochondrial respiratory inhibitor PA. This glycosidation of PA into GPA lost the inhibitory activity to mitochondrial respiration but gained the inhibitory activity to glucose uptake, which would be informative to chemists to control the inhibitor target between glucose transporter and mitochondrial respiration by a simple glycosidation. Finally, we found that GPA-mediated inhibition of glycolysis dramatically decreases intracellular ATP levels only when mitochondrial respiration is inhibited, and concluded that this ATP decrease caused the synergistic filopodia inhibition by GPA and PA. In the end, this is the first report, to our knowledge, on the novel use of CE-TOFMS metabolomic analysis to isolate the target protein of the natural product inhibitor.

EXPERIMENTAL PROCEDURES

Filopodia Protrusion Assay and ATP Determination

Cells were seeded sparsely at 5 × 10^4 cells ml^{-1} (250 μl per well in 48-well plates. Sparse cell seeding was maintained throughout this study). After 1 day, the growth media was changed to CS 0.2% DMEM and the cells were incubated for 12–18 hr. Cells were then treated with the assay samples for 30 min, followed by stimulation with 30 ng ml^{-1} of EGF (Sigma) for 30 min and observed under microscopy.

For screening, isolation from the broth, and evaluation of compounds, cells with complete absence of filopodia were judged to be filopodia inhibited. To quantify the filopodia cell population, filopodia protrusion was induced in the same manner as above except that cells were seeded on glass coverslips in 12-well plates. The cells formed colonies on the coverslips, and filopodia cell colonies were then counted. Colony counts were done in nine fields chosen at random for one sample.

Cellular ATP levels were determined using an ATP assay kit (Sigma) after cells had been treated for 30 min with test compounds.

For the test of inhibitors of mitochondrial respiration, concentrations of 100 nM rotenone, 10 ng ml^{-1} of antimycin A, and 10 ng ml^{-1} of oligomycins were used.

CE-TOFMS Metabolomics

Cells grown in 100 mm dishes were incubated in serum-reduced media for 18 hr and then treated with test compounds for 30 min. After washing cells twice with ice-cold 5% mannitol, metabolites were extracted by keeping cells resting on ice for 10 min in 1 ml of ice-cold methanol containing internal standards (25 μM each of 3-aminopyrrolidine [Aldrich], L-methionine sulfone [Wako], trimesate [Wako], and MES [Wako]). Extracts were then transferred to a separate tube and mixed with 500 μl of milli-Q water, and 600 μl of this solution was transferred into another tube, mixed with 400 μl of chloroform, and centrifuged. A 300 μl aliquot of the aqueous layer was centrifugally filtered through a 5 kDa cutoff membrane (Millipore) to remove proteins from samples. The filtrate was lyophilized, dissolved in 50 μl of milli-Q water, and subjected to CE-TOFMS analysis.

For the [^{13}C]-isotope labeling study, culture media was changed to glucose-depleted DMEM after 18 hr incubation in serum-reduced media, and cells were treated with 1 mg ml^{-1} of [1,2,3,4,5,6-^{13}C]-glucose (Isotec) immediately after the test compounds addition. Metabolites were extracted after 30 min. For the clear measurement of glucose-6-phosphate, fructose-6-phosphate, and glucose-1-phosphate, LC-MS systems were also used. Details of the metabolomic analysis are discussed in Supplemental Experimental Procedures.

In Vitro Hexokinase Assay

Hexokinase is very active when the enzyme is bound to mitochondria (Floridi et al., 1981); therefore, hexokinase was isolated from crude mitochondria as described by Floridi et al., with minor modifications.

Small fragments of bovine heart in MSH buffer (210 mM mannitol, 70 mM sucrose, 1 mM EGTA, 1 mM DTT, 0.1% BSA and 10 mM HEPES [pH 7.4]) were homogenized with a Dounce Tissue Grinder and centrifuged at 1000 × g for 10 min. The supernatant was further centrifuged at 8000 × g for 20 min. The resulting pellet was homogenized in MSH buffer and centrifuged again. The crude mitochondria pellet was homogenized and stored at −80°C until used.

For the measurement of hexokinase activity, G6PDH (Sigma) was used to generate NADPH from the product of the hexokinase reaction. Hexokinase activity was spectrophotometrically determined from the absorbance of NADPH at 340 nm (Bergmeyer, 1963). The reaction mixture contained 30 μg of bovine heart mitochondria, 1 mM ATP, 0.5 mM $NADP^+$, 2 μM rotenone (Calbiochem), 3 μg ml^{-1} oligomycins (Calbiochem), and 0.1 units of G6PDH in 100 μl of PT buffer (10 mM MOPS, 200 mM sucrose, 5 mM succinate, 1 mM P*i*, and 0.01 mM EGTA [pH 7.4]). The reaction was initiated by addition of 0.2 mM glucose at room temperature after a 10 min preincubation period. The level of NADPH was continuously recorded for 20 min.

Uptake of [^{3}H]-2-Deoxyglucose

Serum-starved A431 cells in DMEM containing 1.2 mM glucose were treated with test compounds along with 0.5 μCi of [1,2-^{3}H]-2-deoxy-D-glucose ([^{3}H]-2DG, specific activity 50–60 Ci mmol^{-1}, ARC) for 30 min, washed twice with ice-cold PBS, and lysed with 0.5 N NaOH. Cell lysate radioactivity was measured on a liquid scintillation counter.

Swiss 3T3-L1 preadipocytes were differentiated into adipocytes as described (Saito et al., 2007). Adipocytes were pretreated with or without insulin (100 nM, Sigma) for 15 min for GLUT4 translocation, and then treated with test compounds and [^{3}H]-2DG for 5 min for the glucose uptake study. Other conditions were the same as described above.

To test GPA sensitivity to GLUT1 overexpression, HEK293T cells were transfected with glut1 (derived from A431 cells) using lipofectamine. In the uptake study, an HEK293T cell suspension was used because the cells are easily detached from the culture plates and it was quite difficult to wash cells immediately to terminate the uptake reaction. After 36 hr from transfection, cells were left in PBS containing 1 mM EDTA for the gentle detachment. A suspension of 2.0 × 10^5 cells in 200 μl of glucose-free DMEM in a tube was treated with test compounds and [^{3}H]-2DG in a 25°C water bath for 5 min. Glucose uptake was terminated by the addition of ice-cold high glucose solution (final 25 mM), followed by centrifugation at 1000 × g at 4°C for 5 min. Cell pellets were washed once with ice-cold high glucose solution and lysed with 0.1 N NaOH. [^{3}H]-2DG uptake under this condition linearly increased for at least 30 min.

SUPPLEMENTAL INFORMATION

Supplemental Information includes four figures, four tables, and Supplemental Experimental Procedures and can be found with this article online at doi:10.1016/j.chembiol.2010.06.017.

ACKNOWLEDGMENTS

We are grateful to K. Kami, Y. Kakazu, and S. Sato (Institute for Advanced Biosciences, Keio University) for technical assistance and advice regarding metabolomic analyses. We also thank Y. Takahashi and R. Sawa (Microbial Chemistry Research Center) for their kind help with the structural elucidation of GPA and PA. We thank M. Igarashi for help with microbial fermentation. M.K. was a research assistant for the Global COE Program for Human Metabolomic Systems Biology. M.I., T.S., and M.K. designed the study, analyzed the data, and wrote the paper. M.K. performed the experiments and analyzed the data, while S.I. performed the metabolome measurements. T.S. performed the metabolomic analysis, and E.T. and T.S. provided critical advice and contributed to writing the paper.

Received: April 8, 2010
Revised: June 18, 2010
Accepted: June 21, 2010
Published: September 23, 2010

REFERENCES

Abel, U., Koch, C., Speitling, M., and Hansske, F.G. (2002). Modern methods to produce natural-product libraries. Curr. Opin. Chem. Biol. *6*, 453–458.

Ahn, S.C., Kim, B.Y., Park, C.S., Lee, H.S., Suh, P.G., Ryu, S.H., Rho, H.M., Rhee, J.S., Mheen, T.I., and Ahn, J.S. (1995). Inhibition of PDGF-induced phosphoinositide-turnover by glucopiericidin A. Biochem. Mol. Biol. Int. *37*, 125–132.

Alaimo, P.J., Shogren-Knaak, M.A., and Shokat, K.M. (2001). Chemical genetic approaches for the elucidation of signaling pathways. Curr. Opin. Chem. Biol. *5*, 360–367.

Aloj, L., Caracó, C., Jagoda, E., Eckelman, W.C., and Neumann, R.D. (1999). Glut-1 and hexokinase expression: relationship with 2-fluoro-2-deoxy-D-glucose uptake in A431 and T47D cells in culture. Cancer Res. *59*, 4709–4714.

Bachelard, H.S., Clark, A.G., and Thompson, M.F. (1971). Cerebral-cortex hexokinase. Elucidation of reaction mechanisms by substrate and dead-end inhibitor kinetic analysis. Biochem. J. *123*, 707–715.

Bacon, C., Lakics, V., Machesky, L., and Rumsby, M. (2007). N-WASP regulates extension of filopodia and processes by oligodendrocyte progenitors, oligodendrocytes, and Schwann cells-implications for axon ensheathment at myelination. Glia *55*, 844–858.

Bergmeyer, H.U. (1963). Methods of Enzymatic Analysis (New York: Verlag Chemie, Academic Press).

Deberardinis, R.J., Mancuso, A., Daikhin, E., Nissim, I., Yudkoff, M., Wehrli, S., and Thompson, C.B. (2007). Beyond aerobic glycolysis: transformed cells can engage in glutamine metabolism that exceeds the requirement for protein and nucleotide synthesis. Proc. Natl. Acad. Sci. USA *104*, 19345–19350.

Faix, J., and Rottner, K. (2006). The making of filopodia. Curr. Opin. Cell Biol. *18*, 18–25.

Fenteany, G., Standaert, R.F., Lane, W.S., Choi, S., Corey, E.J., and Schreiber, S.L. (1995). Inhibition of proteasome activities and subunit-specific amino-terminal threonine modification by lactacystin. Science *268*, 726–731.

Floridi, A., Paggi, M.G., D'Atri, S., De Martino, C., Marcante, M.L., Silvestrini, B., and Caputo, A. (1981). Effect of lonidamine on the energy metabolism of Ehrlich ascites tumor cells. Cancer Res. *41*, 4661–4666.

Gutman, M., Singer, T.P., Beinert, H., and Casida, J.E. (1970). Reaction sites of rotenone, piericidin A, and amytal in relation to the nonheme iron components of NADH dehydrogenase. Proc. Natl. Acad. Sci. USA *65*, 763–770.

Hall, C., Wu, M., Crane, F.L., Takahashi, H., Tamura, S., and Folkers, K. (1966). Piericidin A: a new inhibitor of mitochondrial electron transport. Biochem. Biophys. Res. Commun. *25*, 373–377.

Hart, C.P. (2005). Finding the target after screening the phenotype. Drug Discov. Today *10*, 513–519.

Hirayama, A., Kami, K., Sugimoto, M., Sugawara, M., Toki, N., Onozuka, H., Kinoshita, T., Saito, N., Ochiai, A., Tomita, M., et al. (2009). Quantitative metabolome profiling of colon and stomach cancer microenvironment by capillary electrophoresis time-of-flight mass spectrometry. Cancer Res. *69*, 4918–4925.

Ishii, N., Nakahigashi, K., Baba, T., Robert, M., Soga, T., Kanai, A., Hirasawa, T., Naba, M., Hirai, K., Hoque, A., et al. (2007). Multiple high-throughput analyses monitor the response of E. coli to perturbations. Science *316*, 593–597.

Kovacević, Z., Popović, J., Brkljac, O., and Lelas, S. (1987). Interaction of metabolism of aspartate and inosine and energy state of malignant cells. Biochem. J. *247*, 47–51.

Le Clainche, C., and Carlier, M.-F. (2008). Regulation of actin assembly associated with protrusion and adhesion in cell migration. Physiol. Rev. *88*, 489–513.

Liu, J., Farmer, J.D., Lane, W.S., Friedman, J., Weissman, I., and Schreiber, S.L. (1991). Calcineurin is a common target of cyclophilin-cyclosporin A and FKBP-FK506 complexes. Cell *66*, 807–815.

Lokey, R.S. (2003). Forward chemical genetics: progress and obstacles on the path to a new pharmacopoeia. Curr. Opin. Chem. Biol. *7*, 91–96.

Matsumoto, M., Mogi, K., Nagaoka, K., Ishizeki, S., Kawahara, R., and Nakashima, T. (1987). New piericidin glucosides, glucopiericidins A and B. J. Antibiot. (Tokyo) *40*, 149–156.

Mattila, P.K., and Lappalainen, P. (2008). Filopodia: molecular architecture and cellular functions. Nat. Rev. Mol. Cell Biol. *9*, 446–454.

Molitoris, B.A., Geerdes, A., and McIntosh, J.R. (1991). Dissociation and redistribution of Na+,K(+)-ATPase from its surface membrane actin cytoskeletal complex during cellular ATP depletion. J. Clin. Invest. *88*, 462–469.

Monton, M.R.N., and Soga, T. (2007). Metabolome analysis by capillary electrophoresis-mass spectrometry. J. Chromatogr. A *1168*, 237–246, discussion 236.

Mueckler, M., Caruso, C., Baldwin, S.A., Panico, M., Blench, I., Morris, H.R., Allard, W.J., Lienhard, G.E., and Lodish, H.F. (1985). Sequence and structure of a human glucose transporter. Science *229*, 941–945.

Newman, D.J., and Cragg, G.M. (2007). Natural products as sources of new drugs over the last 25 years. J. Nat. Prod. *70*, 461–477.

Pandey, A., and Mann, M. (2000). Proteomics to study genes and genomes. Nature *405*, 837–846.

Parlo, R.A., and Coleman, P.S. (1984). Enhanced rate of citrate export from cholesterol-rich hepatoma mitochondria. The truncated Krebs cycle and other metabolic ramifications of mitochondrial membrane cholesterol. J. Biol. Chem. *259*, 9997–10003.

Piva, T.J., and McEvoy-Bowe, E. (1998). Oxidation of glutamine in HeLa cells: role and control of truncated TCA cycles in tumour mitochondria. J. Cell. Biochem. *68*, 213–225.

Rabinovitz, I., Toker, A., and Mercurio, A.M. (1999). Protein kinase C-dependent mobilization of the alpha6beta4 integrin from hemidesmosomes and its association with actin-rich cell protrusions drive the chemotactic migration of carcinoma cells. J. Cell Biol. *146*, 1147–1160.

Saito, T., Jones, C.C., Huang, S., Czech, M.P., and Pilch, P.F. (2007). The interaction of Akt with APPL1 is required for insulin-stimulated Glut4 translocation. J. Biol. Chem. *282*, 32280–32287.

Scheepers, A., Joost, H.G., and Schurmann, A. (2004). The glucose transporter families SGLT and GLUT: molecular basis of normal and aberrant function. JPEN J. Parenter. Enteral Nutr. *28*, 364–371.

Shulman, Z., Shinder, V., Klein, E., Grabovsky, V., Yeger, O., Geron, E., Montresor, A., Bolomini-Vittori, M., Feigelson, S.W., Kirchhausen, T., et al. (2009). Lymphocyte crawling and transendothelial migration require chemokine triggering of high-affinity LFA-1 integrin. Immunity *30*, 384–396.

Soga, T., Ohashi, Y., Ueno, Y., Naraoka, H., Tomita, M., and Nishioka, T. (2003). Quantitative metabolome analysis using capillary electrophoresis mass spectrometry. J. Proteome Res. *2*, 488–494.

Soga, T., Baran, R., Suematsu, M., Ueno, Y., Ikeda, S., Sakurakawa, T., Kakazu, Y., Ishikawa, T., Robert, M., Nishioka, T., et al. (2006). Differential metabolomics reveals ophthalmic acid as an oxidative stress biomarker indicating hepatic glutathione consumption. J. Biol. Chem. *281*, 16768–16776.

Sugimoto, M., Wong, D., Hirayama, A., Soga, T., and Tomita, M. (2009). Capillary electrophoresis mass spectrometry-based saliva metabolomics identified oral, breast and pancreatic cancer-specific profiles. Metabolomics *6*, 78–95.

Witke, W. (2004). The role of profilin complexes in cell motility and other cellular processes. Trends Cell Biol. *14*, 461–469.

Zheng, X.F.S., and Chan, T.-F. (2002). Chemical genomics in the global study of protein functions. Drug Discov. Today *7*, 197–205.

The Journal of Antibiotics (2010) 63, 601–605

www.nature.com/ja

ORIGINAL ARTICLE

Isolation and structure elucidation of a novel androgen antagonist, arabilin, produced by *Streptomyces* sp. MK756-CF1

Tatsuro Kawamura[1,3], Takahiro Fujimaki[1,3], Natsuki Hamanaka[1], Kentaro Torii[1], Hiroki Kobayashi[1], Yoshikazu Takahashi[2], Masayuki Igarashi[2], Naoko Kinoshita[2], Yoshio Nishimura[2], Etsu Tashiro[1] and Masaya Imoto[1]

In the course of screening for a new type of androgen receptor (AR) antagonist, we isolated a novel compound, arabilin, with two structural isomers, spectinabilin and SNF4435C, produced by *Streptomyces* sp. MK756-CF1. Structure elucidation on the basis of the spectroscopic properties showed that arabilin is a novel polypropionate-derived metabolite with a *p*-nitrophenyl group and a substituted γ-pyrone ring. Arabilin competitively blocked the binding of androgen to the ligand-binding domain of AR *in vitro*. In addition, arabilin inhibited androgen-induced prostate-specific antigen mRNA expression in prostate cancer LNCaP cells.
The Journal of Antibiotics (2010) **63,** 601–605; doi:10.1038/ja.2010.98; published online 25 August 2010

Keywords: androgen antagonist; prostate cancer; PSA

INTRODUCTION

Androgen receptor (AR), a member of the nuclear receptor superfamily, is a critical mediator of prostate cancer; therefore, treatment with AR antagonists is expected to be an effective prostate cancer therapy. AR antagonists can be classified into two structural types, steroidal and nonsteroidal compounds.[1,2] Steroidal AR antagonists often exhibit side effects because of cross-reactivity with other steroid hormone nuclear receptors, such as estrogen receptor and progesterone receptor. On the other hand, anilide-type compounds, such as flutamide and bicalutamide, are representative of nonsteroidal AR antagonists. Although these anilide-type AR antagonists have been clinically used for prostate cancer therapy, prostate cancer often advances to a hormone-refractory state after long-term treatment with AR antagonists.[3] The mutation in AR is considered a possible reason for rendering prostate cancer cells hormone refractory.[4] Furthermore, anilide-type AR antagonists act as agonists toward hormone-refractory prostate cancer cells in some cases.[5–7] Thus, development of a new type of AR antagonist is an attractive strategy to overcome prostate cancers that are resistant to the known AR antagonists.

In the course of screening for a new type of AR antagonist, we isolated a novel compound, arabilin, with two known structural isomers, spectinabilin and SNF4435C, from *Streptomyces* sp. MK756-CF1. In this paper, the isolation, structure elucidation and biological activities of arabilin are reported.

RESULTS AND DISCUSSION

Screening for binding inhibitors of DHT and AR

To obtain a new type of AR antagonist with a nonsteroidal/nonanilide-type structure, we first screened more than 2000 microbial extracts to find inhibitors, which could inhibit the binding of dihydrotestosterone (DHT) to AR using a [^{3}H]DHT-AR *in vitro* binding assay. In the course of screening, we found that the culture broth extract of strain MK756-CF1 inhibited the binding of DHT to AR.

Taxonomy of the producing strain

Strain MK756-CF1 produced spore chains on aerial mycelia, which developed from branched substrate mycelia. The partial gene sequence (1412 bp) coding 16S ribosomal RNA of MK756-CF1 showed high homology with those of members of the genus *Streptomyces*, such as *Streptomyces spectabilis* (National Institute of Technology and Evaluation Biological Research Center (NBRC) 13423T 1408/1413 bp, 99%) and *Streptomyces flavofungini* (NBRC 13371T 1391/1412 bp, 98%). These phenotypic and genotypic properties suggested that strain MK756-CF1 belonged to the genus *Streptomyces*. Further detailed taxonomic study of strain MK756-CF1 is in progress.

Isolation of arabilin, spectinabilin and SNF4435C

The cultivation of strain MK756-CF1 was carried out in 60 500-ml Erlenmeyer flasks containing pressed wheat (2.4 kg) because this solid-state fermentation enabled the strain to produce abundant active

[1]Department of Biosciences and Informatics, Faculty of Science and Technology, Keio University, Yokohama, Japan and [2]Institute of Microbial Chemistry, Tokyo, Japan
[3]These authors contributed equally to this work.
Correspondence: Professor M Imoto, Department of Biosciences and Informatics, Keio University, 3-14-1 Hiyoshi Kohoku-ku, Yokohama, Kanagawa, 223-8522, Japan.
E-mail: imoto@bio.keio.ac.jp
Received 15 June 2010; revised 15 July 2010; accepted 21 July 2010; published online 25 August 2010

components. After fermentation, the culture was extracted with EtOH (2 l), filtrated and concentrated *in vacuo*. This suspension was adjusted to pH 7.0, followed by extraction with EtOAc (3 l) twice, and the organic layer was concentrated to give a pink oily residue (2.2 g). Thus, the obtained crude active oil was subsequently subjected to silica gel column chromatography (Silica gel 60, 60–230 μm; Merck, Darmstadt, Germany) using an *n*-hexane-EtOAc stepwise system. One active fraction (*n*-hexane-EtOAc, 2:1) was further purified by preparative octadecyl silyl (ODS) HPLC (Sun Fire, 10 μm, 19×250 mm; Waters, Milford, MA, USA) with 80% aqueous MeOH to give a pure novel compound, arabilin (3.3 mg) (Figure 1). Another active fraction obtained by silica gel column chromatography (*n*-hexane-EtOAc, 1:1) was also further purified by preparative ODS HPLC to give spectinabilin (3.0 mg)[8] and SNF4435C (6.0 mg)[9] (Figure 1). Spectinabilin and SNF4435C were reported as a weak inhibitor of Rauscher leukemia virus reverse transcriptase[8] and a potent immunosuppressant,[9] respectively.

Structure elucidation of arabilin

The physicochemical properties of arabilin, as well as spectinabilin and SNF4435C, are summarized in Table 1.[8,10] From HRESI-MS measurements in combination with ^{1}H and ^{13}C NMR data, the molecular formula of arabilin was determined to be $C_{28}H_{31}NO_6$ (found: 478.2215 $[M+H]^+$, calcd: 478.2224), the same as spectinabilin and SNF4435C. As the ^{1}H and ^{13}C NMR spectra of arabilin were partially similar to those of spectinabilin,[8,11] a structural study of arabilin was performed by comparing with spectinabilin. The IR spectrum revealed that arabilin possesses a ketone conjugated with a double bond (1666 cm^{-1}) and a nitro group (1516 and 1342 cm^{-1}), as does spectinabilin. On the other hand, the UV spectrum of arabilin (λ_{max}: 263 nm (ε 18 400), 315 nm (sh, ε 10 300)) was different from that of spectinabilin (λ_{max}: 252 nm (ε 17 600), 268 nm (ε 18 200), 367 nm (ε 15 500)).[8] The structure of arabilin was mainly determined by NMR spectral analyses as follows. We established direct connectivity

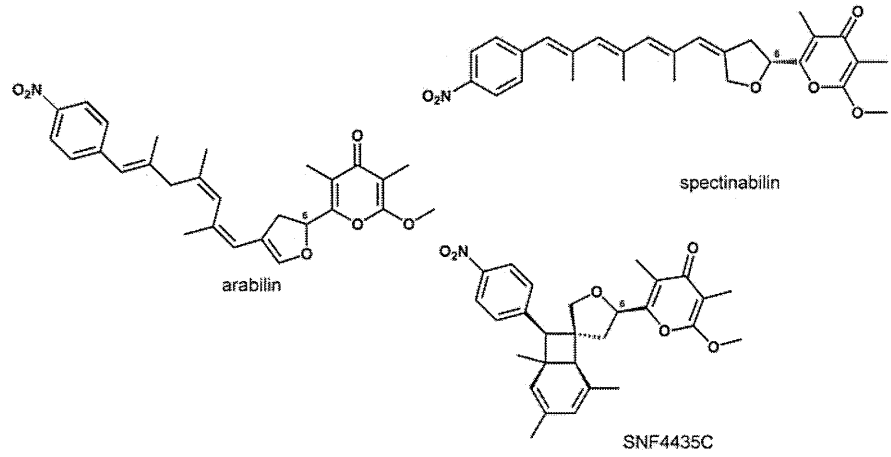

Figure 1 Structures of arabilin, spectinabilin and SNF4435C.

Table 1 Physicochemical properties of arabilin, spectinabilin and SNF4435C

	Arabilin	*Spectinabilin*	*SNF4435C*
Appearance	Pale yellow powder	Pale yellow powder	Pale yellow powder
Molecular formula	$C_{28}H_{31}NO_6$	$C_{28}H_{31}NO_6$	$C_{28}H_{31}NO_6$
Molecular weight	477	477	477
HRESI-MS (m/z, Positive)			
Calcd	478.2224 (as $C_{28}H_{32}NO_6$)	—	—
Found	478.2215	—	—
Optical rotation $[\alpha]_D$	−166.2°	+60.6° [a]	−105.6° [b]
	(*c* 0.13, $CHCl_3$, 25°C)	(*c* 5.0, $CHCl_3$, 26°C)	(*c* 0.1, $CHCl_3$, 26°C)
IR V_{max} (cm^{-1}) (KBr)	2956, 2854, 1666, 1597, 1516, 1342	1670, 1520, 1340[a]	2950, 2850, 1695, 1600, 1520, 1350[b]
UV λ_{max} (nm) (ε)	263 (18400), 315 (sh, 10300) (MeOH)	218 (19100), 252 (17600), 268 (18200), 367 (15500) (EtOH)[a]	271 (19300) (MeOH)[b]
TLC (R_F)[c]	0.68	0.51	0.55
HPLC (Rt, min)[d]	25.2 (85% MeOH)	23.5 (85% MeOH)	16.7 (85% MeOH)
Solubility			
Soluble	$CHCl_3$, MeOH	$CHCl_3$, MeOH	$CHCl_3$, MeOH
Insoluble	*n*-hexane, H_2O	*n*-hexane, H_2O	*n*-hexane, H_2O

[a]Kakinuma *et al.*[8]
[b]Takahashi K. *et al.*[10]
[c]Silica gel TLC (Kieselgel $60F_{254}$; Merck); mobile phase, *n*-hexane-EtOAc (1:2).
[d]Column, SunFire ODS (Waters, 5 μm, 4.6×250 mm); mobile phase, aqMeOH; flow rate, 0.7 ml min^{-1}.

between each proton and carbon by the heteronuclear multiple quantum coherence (HMQC) spectrum; the ^{1}H and ^{13}C spectral data for arabilin are shown in Table 2. The ^{1}H-^{1}H COSY and Heteronuclear Multiple Bond Coherence (HMBC) spectra proved that arabilin has both a 2-methoxy-3,5-dimethyl-γ-pyrone moiety (C-1 to C-5) and a *p*-nitrophenyl group (C-16 to C-19), as does spectinabilin (Figure 2 and Jacobsen *et al.*[11]). This finding and the difference between the UV spectrum of arabilin and that of spectinabilin imply that the tetraene moiety combined with a substituted furan moiety in spectinabilin is not preserved in arabilin. In the ^{1}H NMR spectra, one singlet methylene signal (δ_H 2.91, H-13, 2H) was observed only in arabilin (Table 2 and Jacobsen *et al.*[11]). In the HMBC spectrum of arabilin, ^{1}H–^{13}C long-range couplings from two methyl protons (δ_H 1.73, H-12a and δ_H 1.81, H-14a) to an sp^3 carbon (δ_C 44.2, C-13) were observed (Figure 2), whereas no ^{1}H-^{13}C long-range coupling from the methyl proton to sp^3 carbon was observed in that of spectinabilin (data not shown). In addition, ^{1}H–^{13}C long-range couplings from a methine proton (δ_H 6.48, H-8a) to a methine carbon bearing oxygen (δ_C 77.2, C-6), a methylene carbon (δ_C 35.6, C-7) and a quaternary sp^2 carbon (δ_C 114.9, C-8) indicated that C-8 and C-8a are connected by a double bond in arabilin but not in spectinabilin. Thus, the partial structures of arabilin other than a substituted γ-pyrone ring and a *p*-nitrophenyl group (C-5 to C-16) were also determined on the basis of ^{1}H–^{1}H COSY and HMBC analyses (Figure 2). The geometries of C-8/C-8a, C-9/C-10, C-11/C-12 and C-14/C-15 were determined to be *E*, *Z*, *Z* and *E* by NOE observation between H-8a (δ_H 6.48) and H-9 (δ_H 5.91), H-9 and H-10a (δ_H 1.88), H-11 (δ_H 5.99) and H-12a (δ_H 1.73), and H-13 (δ_H 2.91) and H-15 (δ_H 6.32), respectively (Figure 2). From the above findings, the planar structure of arabilin was determined as shown in Figure 1. Thus, it was revealed that all arabilin and its structural isomers, spectinabilin and SNF4435C, had a *p*-nitrophenyl group and a substituted γ-pyrone ring. The configurations at C-6 in spectinabilin, its analog aureothin and SNF4435C were determined as *R*.[12,13] The stereochemistry of arabilin has not yet been determined and is now under study.

Table 2 ^{13}C- and ^{1}H-NMR data for arabilin in $CDCl_3$

Number	*δc (p.p.m.)*	*δ_H (p.p.m.)*
1	162.1	—
1a	55.3	3.92 (3H, s)
2	99.9	—
2a	6.9	1.86 (3H, s)
3	180.6	—
4	119.6	—
4a	9.4	2.02 (3H, s)
5	154.2	—
6	77.2	5.59 (1H, dd, *J*=7.7, 11.0)
7	35.6	2.85 (1H, dd, *J*=7.5, 15.2)
		3.08 (1H, dd, *J*=11.0, 15.2)
8	114.9	—
8a	144.4	6.48 (1H, s)
9	118.5	5.91 (1H, s)
10	131.7	—
10a	25.3	1.88 (3H, bs)
11	128.6	5.99 (1H, s)
12	134.7	—
12a	22.8	1.73 (3H, bd)
13	44.2	2.91 (2H, s)
14	141.1	—
14a	18.1	1.81 (3H, bd)
15	124.9	6.32 (1H, s)
16	145.1	—
17	129.3	7.35 (2H, d, *J*=8.8)
18	123.5	8.17 (2H, d, *J*=8.8)
19	145.9	—

Chemical shifts in p.p.m. from TMS as an internal standard.

Effects of arabilin, spectinabilin and SNF4435C on binding of DHT to AR

Arabilin, spectinabilin and SNF4435C inhibited the binding of DHT to AR in a dose-dependent manner (Figure 3). The IC_{50} values of arabilin, spectinabilin and SNF4435C were 11 μM, 13 μM and 7 μM, respectively, and these inhibitory activities were about 10-fold more

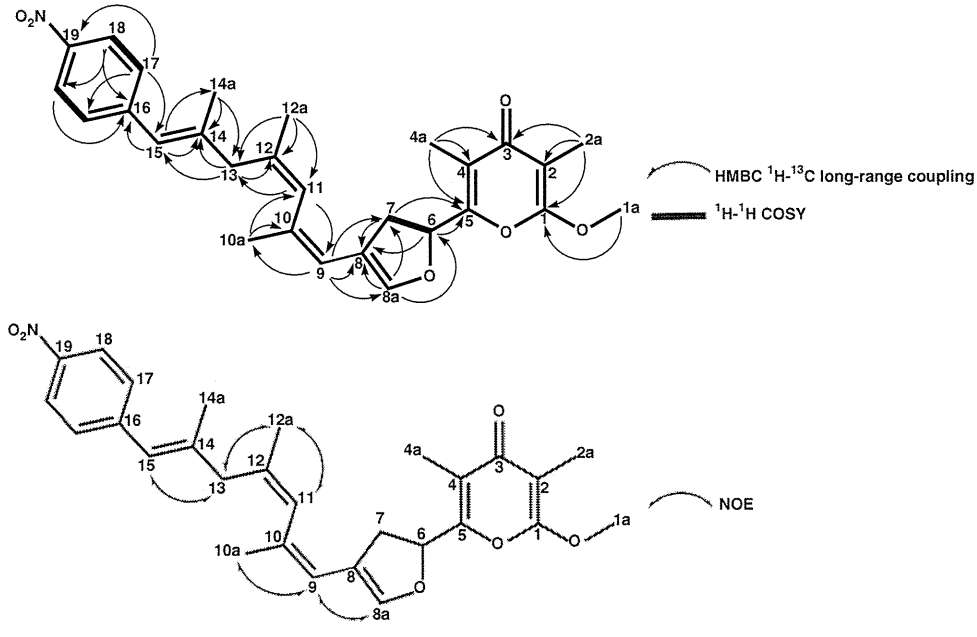

Figure 2 Structures of arabilin elucidated by ^{1}H-^{1}H COSY, NOE and heteronuclear multiple bond coherence (HMBC) experiments.

potent than that of flutamide, which was clinically used for the treatment for prostatic diseases. On the other hand, arabilin, spectinabilin and SNF4435C did not show inhibitory activity against binding of estradiol to estrogen receptor up to 100 μM (data not shown).

Effects of arabilin, spectinabilin and SNF4435C on DHT-induced PSA expression

Prostate-specific antigen (PSA) is a 33-kDa serine protease, whose expression in the prostate is triggered by androgen-mediated action of AR; therefore, to determine whether arabilin, spectinabilin and SNF4435C showed AR antagonistic activity, we examined the effects of these compounds on DHT-induced expression of PSA mRNA in prostate cancer LNCaP cells. As shown in Figure 4, arabilin, spectinabilin and SNF4435C inhibited the DHT-induced expression of endogenous PSA mRNA in LNCaP cells with IC_{50} values of 210 nM, 1.75 nM and 274 nM, respectively, whereas they did not induce the expression of PSA mRNA (data not shown). These three compounds did not inhibit DHT-independent GAPDH gene expression under these conditions (data not shown). Spectinabilin was reported to inhibit *Ascaris* NADH-fumarate reductase,[14] and we found that it inhibited mitochondrial respiration of tumor cells, but its IC_{50} value is about 100 nM. Therefore, inhibition of DHT-induced expression of PSA mRNA by these compounds is not due to nonspecific toxic effect or global RNA synthesis-inhibitory effect, but due to AR antagonistic effect. Thus, we obtained a new type of AR antagonists with non-steroidal/nonanilide-type structures. At present, we do not know why spectinabilin showed 100-fold potent inhibitory activity against DHT-induced PSA mRNA expression when compared with arabilin and SNF4435C. The precise mechanism for the inhibition of DHT-induced PSA mRNA expression by these compounds is now under investigation. In addition, the antitumor activities of these compounds in androgen-dependent and -independent prostate cancer cell functions will be reported elsewhere.

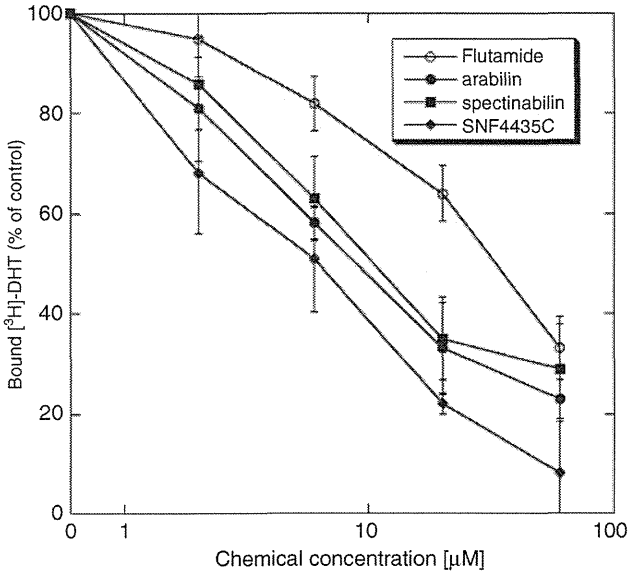

Figure 3 Effects of arabilin, spectinabilin, SNF4435C and flutamide on binding of dihydrotestosterone (DHT) to androgen receptor (AR). A 50 μg ml^{-1} volume of maltose-binding protein-AR-ligand-binding domain (MBP-AR-LBD), 2 nM [^{3}H]DHT and the indicated concentrations of test compounds were incubated at 4°C for 3 h. Then, the radioactivity of [^{3}H]DHT bound to MBP-AR-LBD was measured with a liquid scintillation counter. Values are the means of four samples; bars, s.d.

METHODS

General experimental procedures

Mass spectra were measured with JMS-T100LC mass spectrometer (JEOL, Tokyo, Japan). Optical rotations were made with P-1030 polarimeter (JASCO, Tokyo, Japan) using a micro-cell (light path 100 mm). UV spectra and IR spectra were recorded on U-1800 spectrophotometer (Hitachi High-Technologies, Tokyo, Japan) and FT-210 spectrometer (Horiba, Kyoto, Japan) in KBr disc, respectively. ^{1}H and ^{13}C NMR spectra were recorded on JNM-ECA600 spectrometer (JEOL) operating at 600 MHz and 150 MHz, respectively. A liquid chromatography (LC)-photo diode array (PDA)-MS system (Waters) with a photo diode array detector (2996) and mass analyzer (Micromass ZQ; Waters) was used for analysis and preparation.

Taxonomic studies

The producing strain, MK756-CF1, was isolated from a soil sample collected in Kochi prefecture, Japan. The morphological characteristics of strain

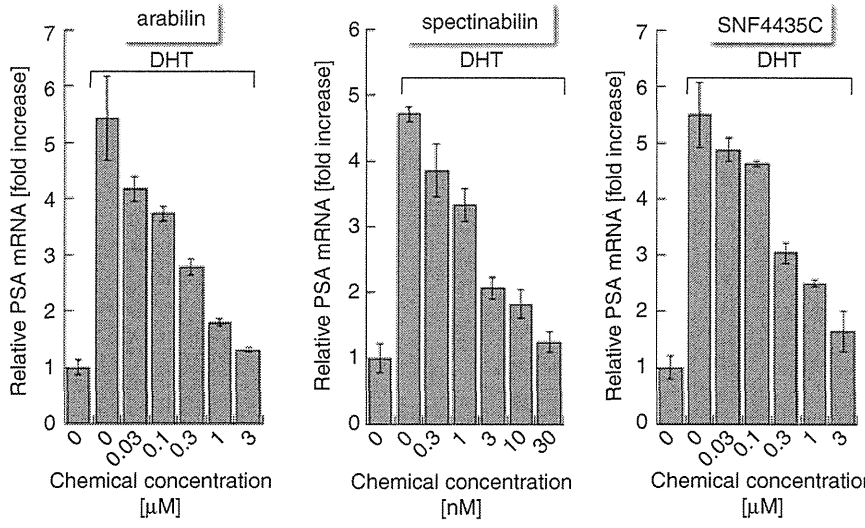

Figure 4 Effects of arabilin, spectinabilin and SNF4435C on dihydrotestosterone (DHT)-induced prostate-specific antigen (PSA) mRNA expression. LNCaP cells were treated with 0.1 nM of DHT and the indicated concentrations of test compounds. After 12 h, PSA mRNA were measured by real-time quantitative reverse transcription PCR. Values are the means of triplicate samples; bars, s.d.

MK756-CF1 were determined on yeast-starch agar. The 16S ribosomal RNA gene was amplified by PCR using genomic DNA of the strain and sequenced. The most related sequences were searched using the BLAST algorithm in the DNA Data Bank of Japan.

Fermentation

A slant culture of arabilin-producing organism was inoculated in a 500-ml baffled Erlenmeyer flask containing 110 ml of a seed medium consisting of galactose 2%, dextrin 2%, Bacto-soytone (Difco; BD, Franklin Lakes, NJ, USA) 1.0%, corn steep liquor (Oji Cornstarch, Tokyo, Japan) 0.5%, $(NH_4)_2SO_4$ 0.2% and $CaCO_3$ 0.2% in deionized water (pH 7.4 before sterilization). The culture was incubated on a rotary shaker (180 r.p.m.) at 27°C for 3 days. The seed culture (7 ml) of the strain was transferred into a 500-ml Erlenmeyer flask containing autoclaved press wheat (15 g) with deionized water (25 ml). The fermentation was carried out by a solid-state cultivation at 30°C for 14 days.

[^{3}H] DHT-AR *in vitro* binding assay

This assay was performed according to the method described previously.[15] In brief, the gene sequence corresponding to the ligand-binding domain (AR-LBD, 609–919 amino acids) in the C-terminus of AR was expressed in *Escherichia coli* strain DH5α as a maltose-binding protein-fused protein (MBP-AR-LBD), followed by purification using amylose resin (Bio-Rad Laboratories, Hercules, CA, USA). Thus, the obtained recombinant MBP-AR-LBD (50 μg ml^{-1}), [^{3}H]DHT (2 nM) and test samples were incubated at 4°C for 3 h. Then, [^{3}H]DHT-bound MBP-AR-LBD was precipitated with hydroxyapatite and radioactivity was measured with a liquid scintillation counter.

Detection of PSA mRNA by real-time reverse transcription PCR

Prostate cancer (LNCaP) cells were incubated in RPMI 1640 medium supplemented with 2% charcoal-stripped serum for 24 h. The cells were then treated with DHT (0.1 nM) and test compounds. After 12 h, RNA from the cells was isolated, and the expression of PSA genes was determined by real-time quantitative reverse transcription PCR, and normalized to GAPDH mRNA. The primer sequences used were as follows: for PSA, 5′-AGGTCGGAGTCAAC GGATTT-3′ (forward) and 5′-TAGTTGAGGTCAATGAAGGG-3′ (reverse); for GAPDH, 5′-GGTCCTCACAGCTGCCCATC-3′ (forward) and 5′-CAGCCTGA GGCGTAGCAGGT-3′ (reverse).

ACKNOWLEDGEMENTS

This study was partly supported by grants from the Ministry of Education, Culture, Sports, Science and Technology of Japan.

1 Gao, W. & Dalton, J. T. Expanding the therapeutic use of androgens via selective androgen receptor modulators (SARMs). *Drug Discov. Today* **12,** 241–248 (2007).
2 Gao, W., Bohl, C. E. & Dalton, J. T. Chemistry and structural biology of androgen receptor. *Chem. Rev.* **105,** 3352–3370 (2005).
3 Scher, H. I., Steineck, G. & Kelly, W. K. Hormone-refractory (D3) prostate cancer: refining the concept. *Urology* **46,** 142–148 (1995).
4 Taplin, M. E. *et al.* Androgen receptor mutations in androgen-independent prostate cancer: Cancer and Leukemia Group B Study 9663. *J. Clin. Oncol.* **21,** 2673–2678 (2003).
5 Steketee, K. *et al.* Broadened ligand responsiveness of androgen receptor mutants obtained by random amino acid substitution of H874 and mutation hot spot T877 in prostate cancer. *Int. J. Cancer.* **100,** 309–317 (2002).
6 Hara, T. *et al.* Novel mutations of androgen receptor: a possible mechanism of bicalutamide withdrawal syndrome. *Cancer Res.* **63,** 149–153 (2003).
7 Yoshida, T. *et al.* Antiandrogen bicalutamide promotes tumor growth in a novel androgen-dependent prostate cancer xenograft model derived from a bicalutamide-treated patient. *Cancer Res.* **65,** 9611–9616 (2005).
8 Kakinuma, K., Hanson, C. A. & Rinehart, K. L. Jr. Spectinabilin, a new nitro-containing metabolite isolated from *Streptomyces spectabilis. Tetrahedron* **32,** 217–222 (1976).
9 Kurosawa, K., Takahashi, K. & Tsuda, E. SNF4435C and D, novel immunosuppressants produced by a strain of *Streptomyces spectabilis.* I. Taxonomy, fermentation, isolation and biological activities. *J. Antibiot.* **54,** 541–547 (2001).
10 Takahashi, K., Tsuda, E. & Kurosawa, K. SNF4435C and D, novel immunosuppressants produced by a strain of Streptomyces spectabilis. II. Structure elucidation. *J. Antibiot.* **54,** 548–553 (2001).
11 Jacobsen, M. F., Moses, J. E., Adlington, R. M. & Baldwin, J. E. The total synthesis of spectinabilin and its biomimetic conversion to SNF4435C and SNF4435D. *Org. Lett.* **7,** 2473–2476 (2005).
12 Ishibashi, Y., Nishiyama, S., Shizuri, Y. & Yamamura, S. Total synthesis of (+)-isoaureothin: determination of the absolute configurations of aureothin, isoaureothin and spectinabilin. *Tetrahedron Lett.* **33,** 521–524 (1992).
13 Parker, K. A. & Lim, Y. H. 'Endo' and 'exo' bicyclo[4.2.0]-octadiene isomers from the electrocyclization of fully substituted tetraene models for SNF 4435C and D. control of stereochemistry by choice of a functionalized substituent. *Org. Lett.* **6,** 161–164 (2004).
14 Ui, H. *et al.* Verticipyrone, a new NADH-fumarate reductase inhibitor, produced by *Verticillium* sp. FKI-1083. *J. Antibiot.* **59,** 785–790 (2006).
15 Nagamine, N. *et al.* Integrating statistical predictions and experimental verifications for enhancing protein-chemical interaction predictions in virtual screening. *PLoS Comput. Biol.* **5,** e1000397 (2009).

The Journal of Antibiotics (2010) 63, 245–250

www.nature.com/ja

ORIGINAL ARTICLE

Terpenoids produced by actinomycetes: isolation, structural elucidation and biosynthesis of new diterpenes, gifhornenolones A and B from *Verrucosispora gifhornensis* YM28-088

Masato Shirai[1], Masaaki Okuda[1], Keiichiro Motohashi[1], Masaya Imoto[2], Kazuo Furihata[3], Yoshihide Matsuo[4,6], Atsuko Katsuta[5], Yoshikazu Shizuri[5] and Haruo Seto[1]

New terpenoids named gifhornenolones A (1) and B (2) were isolated from the culture broth of *Verrucosispora gifhornensis* YM28-088, and their structures were established as hydroxylated isopimaradiene derivatives on the basis of extensive NMR and MS spectral analyses. In addition, a known sesquiterpene compound cyperusol C (3) was isolated. The absolute configuration of 1 was determined by nuclear Overhauser effect spectroscopy (NOESY) and CD spectra as 4*R*, 5*S*, 9*R*, 10*S*, 13*R*, and that of 2 was determined by NOESY experiments as 3*R*, 4*R*, 5*R*, 9*R*, 10*S*, 13*R*. Labeling experiments with [1-^{13}C]glucose and [*U*-$^{13}C_6$]glucose confirmed that the MEP (2-*C*-methyl-D-erythritol-4-phosphate) pathway was used for the biosynthesis of terpenoids in this organism. 1 showed potent inhibitory activity to the androgen receptor with an IC_{50} of 2.8 μg ml^{-1}.
The Journal of Antibiotics (2010) **63,** 245–250; doi:10.1038/ja.2010.30; published online 9 April 2010

Keywords: androgen receptor binding inhibitor; biosynthesis; cyperusol C; gifhornenolone; terpenoid; *Verrucosispora gifhornensis*

INTRODUCTION

Marine microorganisms capable to produce secondary metabolites, marine actinomycetes, in particular, are an attractive resource for screening for bioactive compounds. Indeed, novel compounds exhibiting antitumor and/or antibacterial activity have been isolated from marine actinomycetes.[1] For instance, abyssomicin C isolated from *Verrucosispora* sp. showed antibacterial activity against Gram-positive bacteria including pathogenic *Staphylococcus aureus* strains as an inhibitor of the *para*-aminobenzoic acid biosynthesis pathway.[2–4] In addition, proximicin A produced by the same strain was reported to show antitumor activities.[5,6] Examples of bioactive metabolites isolated from the genus *Verrucosispora* were, however, quite limited presumably due to limited distribution of the genus *Verrucosispora* in the marine environment.

Previously, we carried out screening for terpenoids produced by actinomycetes and succeeded in isolation of several new derivatives such as oxaloterpins[7] and napyradiomycins.[8] In continuation of our work on the isolation of terpenoids of actinomycetes origin,[9] we attempted to obtain terpenoids from the genus *Verrucosispora*. Because terpenoids are lipophilic in most case, we analyzed crude solvent extracts of fermentation broths of several strains of this genus and succeeded in the isolation of two new diterpenoids named gifhornenolones A (**1**) and B (**2**) together with a known compound, cyperusol C (**3**) (Figure 1) from *Verrucosispora gifhornensis* YM28-088.

RESULTS AND DISCUSSION

Fermentation, extraction and isolation

V. gifhornensis YM28-088 that was isolated from an ascidian collected in Hiroshima, Japan, was cultured at 28 °C for 5 days by rotary shaking in 500 ml baffled Erlenmeyer flasks containing 100 ml of the culture medium. The broth was filtered and the broth filtrate was extracted with ethyl acetate (EtOAc). After removal of the solvent, we analyzed the residue extracted with EtOAc by thin layer chromatography (TLC) (*n*-hexane-EtOAc (1:1) or $CHCl_3$-MeOH (10:1), visualized by staining with vanillin-H_2SO_4). Spots appearing bright purple or violet on the TLC plate were selected as potential candidates for isolation. The mycelial cake was extracted with 60% aqueous acetone, and after removal of the solvent, the residual solution was extracted EtOAc and analyzed by TLC in the same manner as above.

[1]Department of Applied Biology and Chemistry, Faculty of Applied Bioscience, Tokyo University of Agriculture, Setagaya-ku, Tokyo, Japan; [2]Faculty of Science and Technology, Keio University, Yokohama-shi, Kanagawa, Japan; [3]Graduate School of Agricultural and Life Sciences, University of Tokyo, Bunkyo-ku, Tokyo, Japan; [4]Marine Biotechnology Institute Co. Ltd., Heita, Kamaishi-shi, Iwate, Japan and [5]Marine Biosciences, Kamaishi Research Laboratory, Kitasato University, Heita, Kamaishi, Iwate, Japan
[6]Current address: Suntory Holdings Limited, R&D Planning Division, Wakayamadai, Shimamoto-cho, Mishima-gun, Osaka, 618-8503, Japan.
Correspondence: Professor Haruo Seto, Department of Applied Biology and Chemistry, Faculty of Applied Bioscience, Tokyo University of Agriculture, Setagaya-ku, Tokyo 156-8502, Japan.
E-mail: haseto@nodai.ac.jp
Received 21 January 2010; revised 5 March 2010; accepted 8 March 2010; published online 9 April 2010

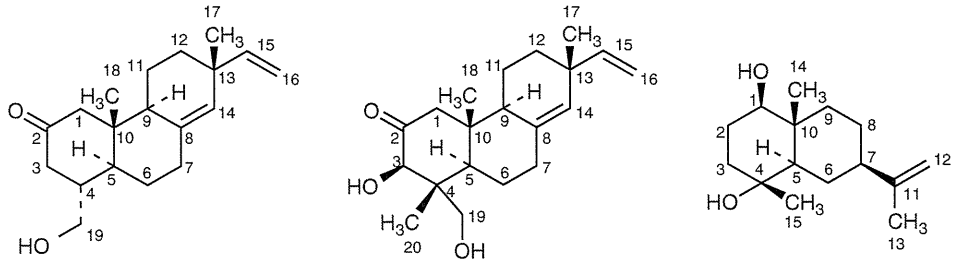

gifhornenolone A (1) gifhornenolone B (2) cyperusol C (3)

Figure 1 The structures of gifhornenolones A (**1**) and B (**2**), and cyperusol C (**3**).

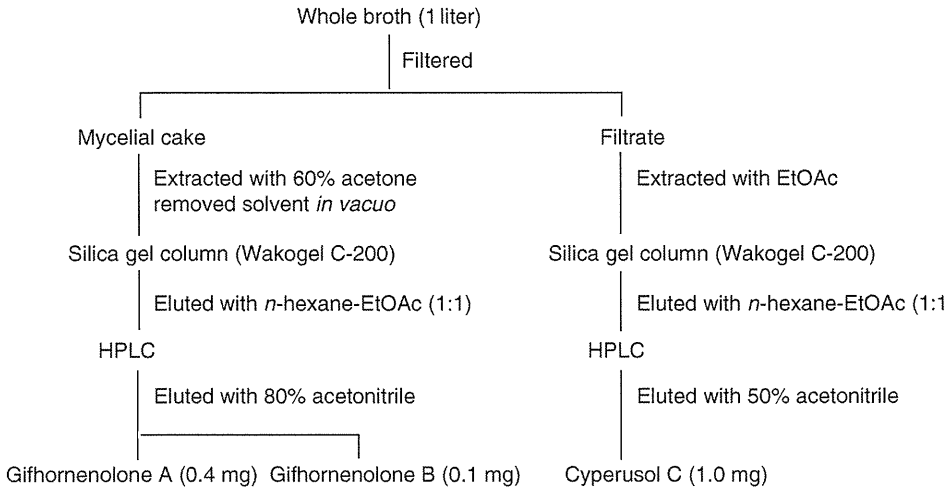

Scheme 1 Isolation and purification of gifhornenolones A (**1**) and B (**2**), and cyperusol C (**3**).

Semi-preparative purification of these positive spots was carried out by Si-gel column chromatography and C-18 reverse-phase high-performance liquid chromatography (RP-HPLC) (Scheme 1). The purified samples thus obtained were analyzed by ^{1}H NMR and fractions showing that methyl signals at around δ1.0 were assumed to contain terpenoids[7,8], because almost all terpenoids possess several methyl groups. As a result of this screening, two fractions showing 2 or 3 methyl proton singlets were expected as terpenoids and subjected to detailed NMR analysis. NMR studies including COSY, HSQC and constant time-HMBC[10] (CT-HMBC) experiments, as well as HR-MS and IR, were used to determine the structures of the following terpenoids, gifhornenolones A (**1**) and B (**2**) from the mycelial cake extracts and cyperusol C (**3**) from the broth filtrate (Figure 1). (See Supplementary information for ^{1}H NMR, ^{13}C NMR, COSY, HSQC, CT-HMBC, nuclear Overhauser effect spectroscopy (NOESY), HR-MS, IR, LC-NMR of gifhornenolone A (**1**), B (**2**) and cyperusol C (**3**).)

Structure elucidation

Gifhornenolone A (**1**) was isolated as colorless needles. Its molecular formula was established as $C_{19}H_{28}O_2$ by HR-MS (*m/z* 289.2145 [M + H]$^+$, calcd 289.2168) indicating six degrees of unsaturation. The IR spectrum of **1** showed a ketone group (1701 cm^{-1}) and a hydroxyl group (3421 cm^{-1}) revealing the oxygen containing functionalities in **1**. The ^{13}C NMR and HSQC spectra confirmed the presence of 19 carbons (Table 1), including one ketone (δ_C 210.6 (C-2)), four olefinic carbons (δ_C 148.3 (C-15), 135.4 (C-8), 130.0 (C-14) and 110.6 (C-16)), one oxymethylene carbon (δ_C 63.9 (C-19)), three methine carbons (δ_C 47.8 (C-9), 45.0 (C-5) and 40.9 (C-4)), six methylene carbons (δ_C 53.4 (C-1), 44.2 (C-3), 34.7 (C-7), 34.1 (C-12), 25.2 (C-6) and 19.1 (C-11)), two singlet methyl groups (δ_C 26.2 (C-17) and 14.1 (C-18)) and two quaternary carbons (δ_C 42.8 (C-10) and 37.4 (C-13)). Further structural information on **1** was obtained by analyzing HSQC, CT-HMBC and COSY spectra.

The singlet methyl protons H-17 showed ^{1}H-^{13}C long-range couplings to C-12, C-13, C-14 and C-15, and the singlet methyl protons H-18 were coupled to C-1, C-5, C-9 and C-10 in the CT-HMBC spectrum. Partial structural information around the oxymethylene protons H-19 was obtained by its coupling to C-3, C-4 and C-5. The deshielded methylene protons H-1 and H-3 were connected to the carbonyl carbon by their couplings to C-2. The olefinic proton H-14 was coupled to C-7 and C-9 in addition to the C-8 sp^2 carbon. The exomethylene protons H-16 were coupled to an sp^2 carbon C-15 revealing the presence of a vinyl residue. This partial structure was corroborated by COSY correlations between H-15 and H-16. The quaternary sp^2 carbon C-8 was coupled to H-6, H-7, H-9 and H-11. In addition, COSY correlations were observed between H-19 and H-7 through H-4, H-5 and H-6, and between H-9 and H-12 through H-11. These results revealed the presence of an isopimaradiene skeleton in **1**.

The relative configuration of **1** was established by analysis of proton coupling constants and NOESY experiments as summarized in Figure 3. The stereochemistry at C-4 could not be determined directly by the splitting pattern of H-4 (1.77 p.p.m., m) due to its overlapping with H-6eq (1.77 p.p.m., m). However, H-5 at 1.74 p.p.m. (ddd, J=11.3, 11.3 and 3.5 Hz) gave satisfactory information. This proton was coupled with H-6eq (1.77 p.p.m., m) and H-6ax (1.17 p.p.m., dddd, J=4.5, 11.3, 13.5 and 13.5 Hz). Thus, the coupling constant between H-5 and H-6ax was determined to be 11.3 Hz suggesting H-5 is in axial orientation. The remaining coupling constant J=11.3 Hz

Table 1 ^{13}C- and ^{1}H-NMR spectral data for 1 and 2

		1			2		
C		δ (^{13}C)	δ (^{1}H)	Multiplicity[a]	δ (^{13}C)	δ (^{1}H)	Multiplicity[a]
1	CH_2	53.4	2.15[b]	d (13.1)	51.0	2.24	d (10.0)
	2.42[c]	dd (13.1, 2.3)		2.47	d (10.0)		
2	C	210.6			211.6		
3	CH_2	44.2	2.38[c]	ddd (14.0, 4.5, 2.3)	77.2[d]	4.35	m
			2.46[b]	dd (14.0,12.9)			
4	CH	40.9	1.77	m	49.2[e]		
5	CH	45.0	1.74	ddd (11.3, 11.3, 3.5)	45.2	2.05	dd (10.5, 2.5)
6	CH_2	25.2	1.17[b]	dddd (13.5,13.5, 11.3, 4.5)	21.9	1.41	m
			1.77[c]	m		1.64	m
7	CH_2	34.7	2.13[b]	ddd (13.5, 13.5, 2.0)	35.0	2.11[b]	m
			2.29[c]	ddd (13.5, 4.5, 2.0)		2.26[c]	ddd (12.0, 4.0, 1.5)
8	C	135.4			135.3		
9	CH	47.8	2.00	dd (7.6, 7.6)	50.2	2.01	dd (6.5, 6.5)
10	C	42.8			44.8		
11	CH_2	19.1	1.50, 1.54	m	18.8	1.50, 1.54	m
12	CH_2	34.1	1.40[b]	ddd (15.0, 11.0, 4.0)	34.1	1.37	ddd (14.0, 11.0, 3.5)
			1.43[c]	m		1.43	m
13	C	37.4			37.4		
14	CH	130.0	5.30	br s	130.1	5.24	br s
15	CH	148.3	5.76	dd (17.5, 10.0)	148.3	5.69	dd (15.0, 9.5)
16	CH_2	110.6	4.90	dd (10.0, 1.5)	110.6	4.84	dd (9.5, 1.5),
			4.92	de (17.5, 1.5)		4.85	dd (15.0, 1.5)
17	CH_3	26.2	1.03	s	26.1	0.98	s
18	CH_3	14.1	0.71	s	16.0	0.77	s
19	CH_2	63.9	3.61	dd (11.0, 2.5),	66.0	3.44	d (9.0)
			3.80	dd (11.0, 4.4)		3.49	d (9.0)
20	CH_3				12.9	0.55	s

NMR spectra were taken in $CDCl_3$.
[a]J in Hz.
[b]CH.
[c]C.
[d]Axial.
[e]Equatorial.

of H-5ax was assigned to the coupling with H-4 suggesting the stereochemistry at H-4 to be axial. This conclusion was also supported by the splitting pattern of H-3ax (12.9 and 14.0 Hz, the latter was assigned to geminal coupling to H-3eq).

NOE correlations were observed between H-4 and H-18, H-18 and H-11ax, and H-11ax and H-17 suggesting all these protons to be in axial orientation. In addition, H-5 showed an NOE to H-9.

The absolute configuration of **1** was clarified by measurement of the CD spectrum that exhibited a positive Cotton effect at 289 nm. Application of the octant rule to this positive Cotton effect clearly indicated that the axial methyl group C-18 is located in the upper left back octant. Consequently, the absolute configurations of the stereogenic centers of **1** were established as 4*R*, 5*S*, 9*R*, 10*S*, 13*R*.

The molecular formula of gifhornenolone B (**2**) was established as $C_{20}H_{30}O_3$ by HR-MS measurement (*m/z* 319.2270 $[M + H]^+$, calcd 319.2273). The ^{13}C NMR and HSQC spectra confirmed the presence of 20 carbons in **2**. Its NMR data were similar to those of **1** (Table 1) except for large downfield shifts of the oxymethine carbon (δ_C 77.2 (C-3)) and one quaternary carbon (δ_C 49.2 (C-4)) with appearance of an additional methyl carbon (δ_C 12.9 (C-20)). Further structural information on **2** was obtained by analyzing CT-HMBC and COSY spectra (Figure 2). Assuming the same stereochemistries for the gross structures of **1** and **2**, the stereochemistry at C-3 of **2** was concluded to be *R* by observation of NOE between H-3 and H-5 as shown in Figure 3.

Cyperusol C (**3**) was obtained as a colorless oil. Its NMR spectral data summarized in experimental section were in agreement with those reported for the known compound.[11] The absolute configuration of this compound was confirmed by NOESY experiments and negative optical rotatory dispersion (ORD) spectrum as summarized in Figure 3 as 3*R*, 4*R*, 5*R*, 9*R*, 10*S*, 13*R*. **3** was first purified from a plant *Cyperus longus*, but its isolation from microorganisms has never been reported.

Biosynthesis of isopentenyl diphosphate

Isopentenyl diphosphate, the starting material for the biosynthesis of terpenoids, is known to be biosynthesized mostly through the MEP (2-*C*-methyl-D-erythritol-4-phosphate) pathway[12] with some exceptions through the classical mevalonate pathway in actinomycetes. The latter examples include naphterpin,[13] terpentecin,[14] napyradiomycin[15] and BE-40644[16]. To examine which pathway was used in *V. gifhornensis* YM28-088, we carried out ^{13}C-labeling experiments with **1** and **3**.

Addition of [1-^{13}C]glucose to the fermentation broth of *V. gifhornensis* YM28-088 increased the signal intensities of C-2, C-6, C-11, C-14, C-16, C-17, C-18 and C-19 of **1** by approximately

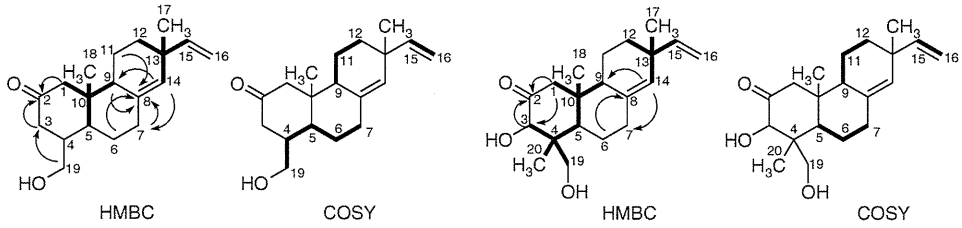

gifhornenolone A (**1**) gifhornenolone B (**2**)

Figure 2 Important ^{1}H-^{13}C CT-HMBC correlations observed for gifhornenolones A (**1**) and B (**2**). Bold lines show HMBC correlations observed with methyl protons, or COSY correlations.

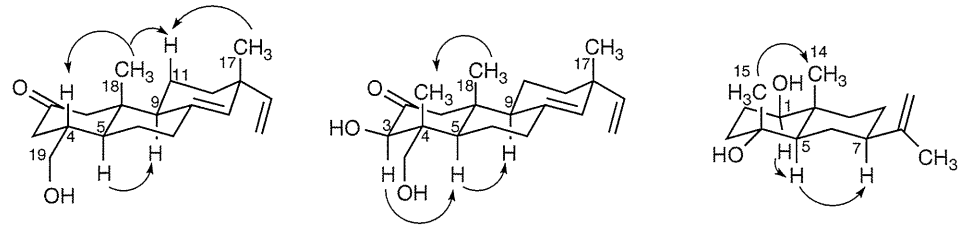

gifhornenolone A (**1**) gifhornenolone B (**2**) cyperusol C (**3**)

Figure 3 NOEs observed for gifhornenolones A (**1**) and B (**2**), and cyperusol C (**3**).

two times (Table 2). In **1** labeled with [*U*-$^{13}C_6$]glucose, eight pairs of ^{13}C-^{13}C couplings were observed between C-2 and C-3, C-4 and C-19, C-5 and C-6, C-8 and C-14, C-9 and C-11, C-10 and C-18, C-13 and C-17, and C-15 and C-16 leaving three enhanced singlet peaks due to C-1, C-7 and C-12. These labeling patterns of **1** were explained by operation of the MEP pathway in *V. gifhornensis* YM28-088 (Figure 4). In agreement with these results, no incorporation of sodium [1-^{13}C]acetate was observed with **1** (data not shown).

Assuming that **2** is a biosynthetic intermediate for **1** and that the carbon skeleton of gifhornenolone is formed by cyclization by chair–chair conformation of geranylgeranyl diphosphate, the biosynthetic scheme for **1** can be summarized as shown in Figure 5. At first, the β-methyl group of **2** is oxidized to carboxylic acid presumably by P450, and then the intermediate is converted to its 2-keto etc. by tautomerization to the 3-keto derivative that is very easily decarboxylated to give an enol derivative. After enolization, we converted the resultant 3-keto intermediate to 2-keto-3-hydroxy derivative by tautomerization. Finally, removal of the alcohol at C-3 may be carried out by dehydration and hydrogenation to give **1**.

In **3**, the signal intensities of C-2, C-6, C-8 and C-13 to 15 were enhanced by about 2.6-fold by the addition of [1-^{13}C]glucose. When labeled with [*U*-$^{13}C_6$]glucose, six pairs of ^{13}C-^{13}C couplings were detected between C-1 and C-2, C-4 and C-15, C-5 and C-6, C-7 and C-8, C-10 and C-14, and C-11 and C-13 with enriched singlet peaks of C-3, C-9 and C-12 (Table 2).

Biological activity

Because isopimarane-type diterpenes have structural similarity to steroidal compounds such as dihydrotestosterone (DHT) and other known androgen antagonists, we expected that **1** might show androgen antagonist activity. **1** showed inhibitory activity against binding of DHT to AR (androgen receptor) with an IC_{50} of 9.7 μM ml^{-1} (*in vitro* binding assay, using [^{3}H]-DHT and recombinant AR).

Table 2 Incorporation of [1-^{13}C]glucose and [U-$^{13}C_6$]glucose into 1 and 3

	1			*3*		
Position	δ_C	*[1-^{13}C]glucose*[a]	*J_{C-C}*[b]	δ_C	*[1-^{13}C]glucose*[a]	*J_{C-C}*[b]
1	53.4	1.0		79.5	1.0	36.5
2	210.6	2.4	38.5	28.6	2.7	36.7
3	44.2	1.1	38.3	40.9	1.0	
4	40.9	1.1	37.7	71.6	1.6	37.4
5	45.0	1.2	34.1	53.0	1.0	34.6
6	25.2	2.3	37.7	25.8	2.6	34.6
7	34.7	1.3		45.7	0.9	32.5
8	135.4	1.0	71.3	26.4	2.7	32.8
9	47.8	0.8	35.6	40.6	1.0	
10	42.8	1.0	36.3	39.0	1.5	36.0
11	19.1	2.4	35.0	150.3	1.5	41.3
12	34.1	1.0		108.4	1.1	
13	37.4	1.1	35.6	21.0	2.6	41.0
14	130.0	2.2	72.2	13.0	2.7	36.1
15	148.3	1.1	69.7	22.8	2.7	37.5
16	110.6	2.3	70.2			
17	26.2	2.0	35.5			
18	14.1	2.0	36.4			
19	63.9	1.9	38.5			

[a]Peak intensities were normalized to C-1 carbon in both the compounds.
[b]Carbon–carbon coupling constants observed with samples labeled by [$^{13}C_6$]glucose.

EXPERIMENTAL SECTION

General experimental procedures

Both 1D ^{1}H and ^{13}C NMR spectra were recorded on a JEOL Alpha 400 NMR spectrometer (JEOL, Akishima, Tokyo, Japan, operating at 400 MHz for ^{1}H and 100 MHz for ^{13}C) or a Varian Inova 500 (Varian, Palo Alto, CA, USA,

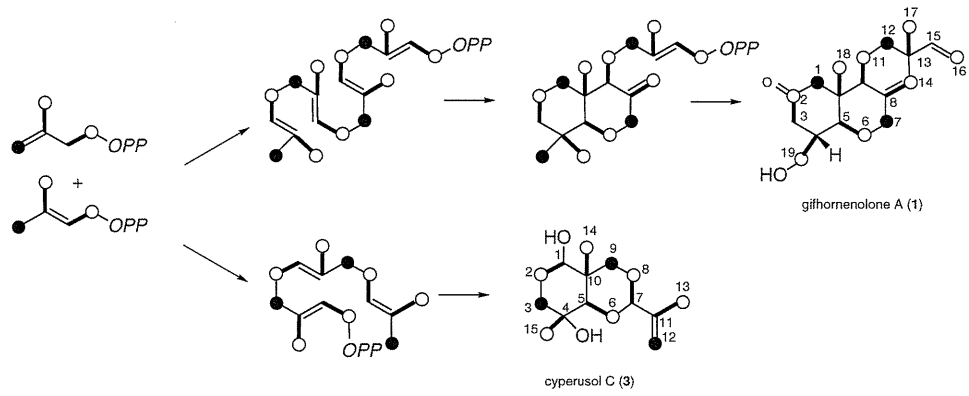

Figure 4 Incorporation patterns of isopentenyl diphosphate (IPP) from [1-^{13}C]glucose and [*U*-$^{13}C_6$]glucose into gifhornenolones A (**1**) and cyperusol C (**3**). Open circles show carbons derived from [1-^{13}C]glucose through the MEP pathway. Closed circles indicate carbons derived from C-3 of pyruvic acid. Bold lines show ^{13}C-^{13}C couplings observed with a sample enriched by [*U*-$^{13}C_6$]glucose.

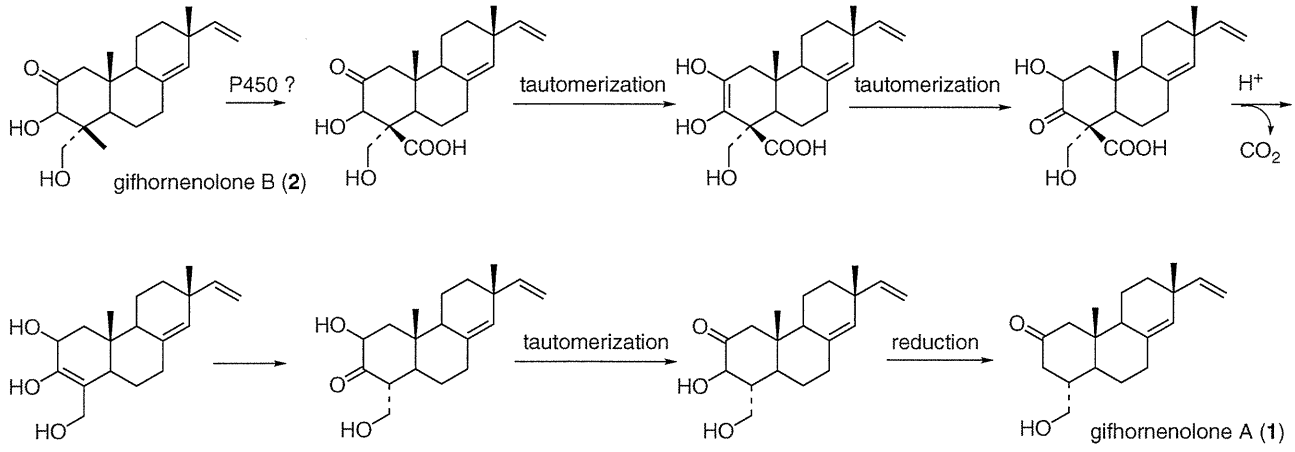

Figure 5 Hypothetical biosynthetic pathway from gifhornenolone B (**2**) to gifhornenolone A (**1**).

operating at 500 MHz for ^{1}H and 125 MHz for ^{13}C). Two-dimensional ^{1}H-^{1}H COSY, NOESY, ^{1}H-^{13}C HSQC, CT-HMBC spectra were recorded on a Varian Inova 500 or JEOL ECA 600 NMR spectrometer. Samples were dissolved in $CDCl_3$ and the solvent peak was used as an internal standard (δ_H 7.24 and δ_C 77.0). HR-ESI-MS data were recorded on a Waters LCT-Premier XE mass spectrometer (Waters, Milford, MA, USA). IR spectra were obtained in KBr with a Shimadzu 8300 FTIR spectrometer (Shimadzu, Kyoto, Japan). Optical rotations were measured on a HORIBA SEPA-300 polarimeter (HORIBA, Kyoto, Japan). CD spectra were recorded on a Jasco J-720WI spectropolarimeter with ORDM-306 attachment (Jasco, Tokyo, Japan). ORD spectra were obtained with a Jasco J-720WI (cylindrical quartz cell ϕ 3.5×100 mm). HPLC purifications were carried out using a SENSHU PAK PEGASIL ODS column (20×250 mm) equipped with a Hitachi High Technologies L-2450 diode array detector (Hitachi, Ibaraki, Japan). Wako Wakogel C-200 was used for Si gel column chromatography (Wako, Osaka, Japan); Si gel 60 F_{254} plastic-backed sheets were used for TLC analysis.

Cultivation of *V. gifhornensis* YM28-088

V. gifhornensis YM28-088 was inoculated with the mycelia of the strain grown on an agar slant into 15 ml test tubes containing 5 ml of a preliminary seed medium consisting of soluble starch 1.0%, polypeptone 1.0%, molasses 1.0% and meat extract 1.0% (pH 7.2 before sterilization), and was cultured at 28 °C for 7 days on a rotary shaker at 170 r.p.m. Aliquot (1 ml) of the seed culture was inoculated into each of 500 ml baffled Erlenmeyer flasks containing 100 ml of the medium consisting of starch 2.0%, polypeptone 0.5%, meat extract 0.5%, dry yeast 0.3% and $CaCO_3$ 0.3% (pH 7.0 before sterilization). The microorganism was cultured at 28 °C for 5 days. This strain is maintained at Marine Biosciences, Kamaishi Research Laboratory, Kitasato University, Heita, Kamaishi, Iwate, Japan.

Purification of gifhornenolones A (1) and B (2)

The fermentation broth (1 liter) was separated into mycelial cake and filtrate by suction filtration. The supernatant was extracted with an equal amount of EtOAc, the organic layer was dried over anhydrous Na_2SO_4 and the solvent was removed under reduced pressure. After mycelial cake was submerged in 60% acetone-water, we removed the solvent under reduced pressure, and extracted the aqueous residue with an equal amount of EtOAc.

The EtOAc extract from the mycelia cake was subjected to Si gel column chromatography (*n*-hexane-EtOAc, 1:1). The eluted fractions were analyzed by color reaction with vanillin-H_2SO_4 on Si gel TLC ($CHCl_3$-MeOH, 10:1). Fractions containing **1** and **2** (Rf 0.4) were combined and further purified by ODS HPLC (20×250 mm; SENSHU PAK PEGASIL ODS) with a PDA detector eluted with CH_3CN in H_2O (80%) at a flow rate of 14 ml min^{-1} to yield **1** (0.4 mg l^{-1}, 9.7 min) and **2** (0.1 mg l^{-1}, 10.1 min).

Gifhornenolone A (**1**). Colorless needles, m.p. 94–95 °C (crystallized from AcOEt—*n*-hexane), $[\alpha]_D^{25}$ +6.6° (*c* 0.18, $CHCl_3$), CD (*c*=1.7, MeOH): $\Delta\varepsilon$=−14.35 (210 nm, neg. max.) $\Delta\varepsilon$=+2.0 (289 nm, pos. max.), IR (KBr) 1701, 3422 cm^{-1}; ^{1}H NMR (400 MHz, $CDCl_3$) and ^{13}C NMR (100 MHz, $CDCl_3$), see Table 1; HR-MS *m/z* 289.2145 (calcd for $C_{19}H_{28}O_2$, [M + H]$^+$ 289.2168).

Gifhornenolone B (**2**). Colorless oil, ^{1}H NMR (400 MHz, $CDCl_3$) and ^{13}C NMR (100 MHz, $CDCl_3$), see Table 1; HR-MS *m/z* 319.2270 (calcd for $C_{19}H_{28}O_2$, $[M + H]^+$ 319.2273).

Purification of cyperusol C (**3**). The EtOAc extract from the filtrate of *V. gifhornensis* YM28-088 was subjected to Si gel column chromatography (*n*-hexane-EtOAc, 1:2). **3** was visualized by color reaction with vanillin-H_2SO_4 on Si gel TLC (*n*-hexane-EtOAc, 1:1). Fractions containing cyperusol C (Rf 0.2) were combined and further purified by ODS HPLC (20×250 mm; SENSHU PAK PEGASIL ODS) with a PDA detector eluted with CH_3CN in H_2O (50%) at a flow rate of 14 ml min^{-1} to yield cyperusol C (1.0 mg l^{-1}, 8.8 min).

Cyperusol C (**3**). Colorless oil, ^{1}H NMR data, δ_H 0.89, 1.12, 1.74 (3H each, s, H_3-14, 15, 13), 1.14 (1H, ddd, *J*=4.0, 13.0, 13.5 Hz, H-9), 1.88 (1H, ddd, *J*=3.5, 3.5, 13.5 Hz, H-9), 1.26, 1.84 (1H each, both m, H-6), 1.28 (1H, m, H-5), 1.38 (1H, dddd, *J*=3.5, 13.0, 13.5, 17.0 Hz, H-8), 1.52 (1H, ddd, *J*=3.5, 12.0, 13.5 Hz, H-3), 1.62 (1H, m, H-8), 1.60, 1.72 (1H each, both m, H-2), 1.80 (1H, ddd, *J*=3.0, 3.5, 12.0 Hz, H-3), 1.92 (1H, m, H-7), 3.34 (1H, dd, *J*=4.4, 11.2 Hz, H-1), 4.70 (2H, m, H_2-12); ^{13}C NMR data, δ_C 79.5 (C-1), 28.6 (C-2), 40.9 (C-3), 71.6 (C-4), 53.0 (C-5), 25.8 (C-6), 45.7 (C-7), 26.4 (C-8), 40.6 (C-9), 39.0 (C-10), 108.4 (C-11), 150.3 (C-12), 21.0 (C-13), 13.0 (C-14), 22.8 (C-15). HR-MS *m/z* 239.2010 (calcd for $C_{19}H_{28}O_2$, $[M + H]^+$ 239.2011).

Biosynthetic experiment

[1-^{13}C]Glucose (1 mg ml^{-1}), sodium [1-^{13}C]acetate (1 mg ml^{-1}) and [*U*-$^{13}C_6$] glucose (1 mg ml^{-1}) were added to the medium 38 h after initiation of the fermentation at separate experiments. Production of **1** and **3** started at about 38 h after cultivation. After 5 days, we purified the labeled samples of **1** and **3** as above, and then subjected them to ^{13}C-NMR NMR spectral analysis.

Biological activity

In vitro AR binding activity was assayed as previously reported with some modifications.[17,18] In brief, 50 μg ml^{-1} recombinant androgen receptor C-termini protein, 2 nM [^{3}H]-DHT and a test compound were mixed in a binding buffer consisting of 50 mM Tris-HCl (pH 7.4), 800 mM NaCl, 10% glycerol, 1 mg ml^{-1} bovine serum albumin and 2 mM DTT to give a 100 μl mixture solution. The mixture was incubated at 4 °C for 3 h, and BioGel HT (Bio-Rad Laboratories, Hercules, CA, USA) was added to the solution and further incubated on ice for 15 min. [^{3}H]-DHT-bound BioGel HT was washed with washing buffer (40 mM Tris-HCl (pH 7.6), 100 mM KCl, 1 mM EDTA and 1 mM EGTA) three times, and its radioactivity was measured by a liquid scintillation counter.

ACKNOWLEDGEMENTS

This work was supported by in part by a Grant-in-Aid for Scientific Research (B) to H Seto. We thank Professor T Ishikawa and Dr T Kumamoto of Chiba University for measurements of CD and ORD spectra. We also thank Dr T Kushiro of University of Tokyo for helpful discussion on the biosynthesis of gifhornenolone.

1 Fenical, W. & Jensen, P. R. Developing a new resource for drug discovery: marine actinomycete bacteria. *Nat. Chem. Biol.* **2,** 666–673 (2006).
2 Bister, B. *et al.* Abyssomicin C—a polycyclic antibiotic from a marine *Verrucosispora* strain as an inhibitor of the *p*-aminobenzoic acid/tetrahydrofolate biosynthesis pathway. *Angew. Chem. Int. Ed.* **43,** 2574–2576 (2004).
3 Riedlinger, J. *et al.* Abyssomicins, inhibitors of the *para*-aminobenzoic acid pathway produced by the marine *Verrucosispora* strain AB-18-032. *J. Antibiot.* **57,** 271–279 (2004).
4 Keller, S. *et al.* Abyssomicins G and H and atrop-abyssomicin C from the marine *Verrucosispora* strain AB-18-032. *J. Antibiot.* **60,** 391–394 (2007).
5 Fiedler, H. P. *et al.* Proximicin A, B and C, novel aminofuran antibiotic and anticancer compounds isolated from marine strains of the Actinomycete. *Verrucosispora J. Antibiot.* **61,** 158–163 (2008).
6 Schneider, K. *et al.* Proximicins A, B, and C—antitumor furan analogues of netropsin from the marine Actinomycete *Verrucosispora* induce upregulation of p53 and the cyclin kinase inhibitor p21. *Angew. Chem. Int. Ed.* **47,** 3258–3261 (2008).
7 Motohashi, K. *et al.* Studies on terpenoids produced by actinomycetes: oxaloterpins A, B, C, D and E, diterpenes from *Streptomyces* sp. KO-3988. *J. Nat. Prod.* **70,** 1712–1717 (2007).
8 Motohashi, K., Sue, M., Furihata, K., Ito, S. & Seto, H. Terpenoids produced by actinomycetes: Napyradiomycins from *Streptomyces antimycoticus* NT17. *J. Nat. Prod.* **71,** 595–601 (2008).
9 Motohashi, K. Studies on terpenoids produced by actinomycetes. 5-Dimethylallylindole-3-carboxylic acid and A80915G-8"-acid produced by marine-derived *Streptomyces* sp. MS239. *J. Antibiot.* **61,** 75–80 (2008).
10 Furihata, K. & Seto, H. Constant time HMBC (CT-HMBC), a new HMBC technique useful for improving separation of cross peaks. *Tetrahedron Lett.* **39,** 7337–7340 (1998).
11 Xu, F., Morikawa, T., Matsuda, H., Ninomiya, K. & Yoshikawa, M. Structures of new sesquiterpenes and hepatoprotective constituents from the Egyptian herbal medicine *Cyperus longus*. *J. Nat. Prod.* **67,** 569–576 (2004).
12 Kuzuyama, T. & Seto, H. Diversity of the biosynthesis of the isoprene units. *Nat. Prod. Rep.* **20,** 171–183 (2003).
13 Shin-ya, K., Furihata, K., Hayakawa, Y. & Seto, H. Biosynthetic studies of naphterpin, a terpenoid metabolite of *Streptomyces*. *Tetrahedron Lett.* **31,** 6025–6026 (1990).
14 Isshiki, K. *et al.* Biosynthesis of terpentecin. *J. Antibiot.* **39,** 1634–1635 (1986).
15 Shiomi, K. *et al.* Biosynthesis of napyradiomycins. *J. Antibiot.* **40,** 1740–1745 (1987).
16 Seto, H., Orihara, N. & Furihata, K. Studies on the biosynthesis of terpenoids produced by actinomycetes. Part 4. Formation of BE-40644 by the mevalonate and nonmevalonate pathways. *Tetrahedron Lett.* **39,** 9497–9500 (1998).
17 Freyberger, A. & Ahr, H. J. Development and standardization of a simple binding assay for the detection of compounds with affinity for the androgen receptor. *Toxicology* **195,** 113–126 (2004).
18 Roselli, C. E. The effect of anabolic-androgenic steroids on aromatase activity and androgen receptor binding in the rat preoptic area. *Brain Res.* **792,** 271–276 (1998).

Supplementary Information accompanies the paper on The Journal of Antibiotics website (http://www.nature.com/ja)

Molecular Microbiology (2010) 76(1), 92–103 ■

doi:10.1111/j.1365-2958.2010.07082.x
First published online 19 February 2010

Distinct subcellular localization in the cytosol and apicoplast, unexpected dimerization and inhibition of *Plasmodium falciparum* glyoxalases

Miriam Urscher,[1] Jude M. Przyborski,[2] Masaya Imoto[3] and Marcel Deponte[1]*

[1]*Butenandt Institute for Physiological Chemistry, Ludwig-Maximilians University, Butenandtstr. 5, D-81377 Munich, Germany.*

[2]*Parasitology, Faculty of Biology, Philipps University Marburg, Karl von Frisch Str. 8, D-35043 Marburg, Germany.*

[3]*Department of Biosciences and Informatics, Faculty of Science and Technology, Keio University, 3-14-1 Hiyoshi, Kohoku-ku, Yokohama 223-8522, Japan.*

Summary

The ubiquitous glyoxalase system removes methylglyoxal as a harmful by-product of glycolysis. Because malaria parasites have drastically increased glycolytic fluxes, they could be highly susceptible to the inhibition of this detoxification pathway. Here we analysed the intracellular localization, oligomerization and inhibition of the glyoxalases from *Plasmodium falciparum*. Glyoxalase I (GloI) and one of the two glyoxalases II (cGloII) were located in the cytosol of the blood stages. The second glyoxalase II (tGloII) was detected in the apicoplast pointing to alternative metabolic pathways. Using a variety of methods, cGloII was found to exist in a monomer–dimer equilibrium that might have been overlooked for homologues from other organisms and that could be of physiological importance. The compounds methylgerfelin and curcumin, which were previously shown to inhibit mammalian GloI, also inhibited *P. falciparum* GloI. Inhibition patterns were predominantly competitive but were complicated because of the two different active sites of the enzyme. This effect was neglected in previous inhibition studies of monomeric glyoxalases I, with consequences for the interpretation of inhibition constants. In summary, the present work reveals novel general glyoxalase properties that future research can build on and provides a significant advance in characterizing the glyoxalase system from *P. falciparum*.

Accepted 28 January, 2010. *For correspondence. E-mail marcel.deponte@gmx.de; Tel. (+49) 89 2180 77122; Fax (+49) 89 2180 77093.

Introduction

Malaria parasites have very high glycolytic fluxes allowing rapid cell division and a drastic increase of parasitemia within several days. Parasitized red blood cells, for example, were found to consume up to 75 times more glucose than uninfected erythrocytes (Sherman, 1979). The degradation of glucose via glycolysis is not a perfect process because of the spontaneous elimination of phosphate from dihydroxyacetone-phosphate or glyceraldehyde-3-phosphate. In mammals and yeast up to 0.4% of triosephosphate isomerase substrate is converted to the toxic by-product methylglyoxal (Thornalley, 1990). Accordingly, the formation of methylglyoxal is thought to be significantly increased in *Plasmodium* species. The compound reacts with physiological nucleophiles resulting in modified nucleic acids and altered/inactivated proteins. Methylglyoxal and other electrophilic 2-oxoaldehydes are therefore removed by the ubiquitous glyoxalase system, yielding D-lactate and other non-toxic 2-hydroxycarboxylic acids (Thornalley, 1990; Thornalley, 1996). Owing to the increased glycolytic fluxes, malaria parasites are predicted to require an efficient detoxification system for harmful methylglyoxal concentrations and could be highly susceptible to glyoxalase inhibition (Vander Jagt *et al.*, 1990; Thornalley, 1990; Akoachere *et al.*, 2005). Indeed, the following studies support the theory that this metabolic pathway could be suited as a drug target.

Using parasite extracts and recombinant enzymes, the human parasite *Plasmodium falciparum* was shown to have a functional glyoxalase system consisting of the isomerase glyoxalase I (GloI), two isozymes of the thioester hydrolase glyoxalase II (cGloII and tGloII) and glutathione (GSH) as a coenzyme (Vander Jagt *et al.*, 1990; Iozef *et al.*, 2003; Akoachere *et al.*, 2005; Deponte *et al.*, 2007; Urscher and Deponte, 2009). Probably because of this efficient detoxification system, D-lactate formation rates from *P. falciparum*-infected erythrocytes